Exotic $Q=-1/3$ quark signatures at high-energy hadron colliders

Troy C. Andre* and Jonathan L. Rosner†
Enrico Fermi Institute and Department of Physics, University of Chicago, Chicago, Illinois 60637, USA
(Received 2 October 2003; published 26 February 2004)

Isosinglet vectorlike quarks are predicted by some unified theories of electroweak and strong interactions. We study hadron collider signatures for the production and decay of isosinglet vectorlike quarks with charge $-1/3$. Previous analyses of run I data from the Fermilab Tevatron are used to set lower limits of 100–200 GeV/c^2 on the mass of such quarks, depending on assumptions about mixing with standard model quarks and the mass of the Higgs boson. For future Tevatron data ($E_{\text{c.m.}}=1.96$ TeV) the corresponding mass range is (100–270, 100–320) GeV/c^2 for (1, 10) fb^{-1}. At the CERN Large Hadron Collider (LHC) ($E_{\text{c.m.}}=14$ TeV, 100 fb^{-1}), an analysis of flavor-changing neutral-current decay modes should probe an h quark mass range of 100–1100 GeV/c^2.

DOI: 10.1103/PhysRevD.69.035009 PACS number(s): 12.10.Dm, 12.15.Ff, 13.85.Rm, 14.65.Fy

I. INTRODUCTION

The currently known fermions consist of quarks (u,c,t) with charge 2/3, quarks (d,s,b) with charge $-1/3$, leptons (e,μ,τ) with charge -1, and neutrinos (ν_e,ν_μ,ν_τ) with charge 0. In the standard model (SM), these fermions are arranged into structures that transform under the gauge group $\mathrm{SU}(3)_c\times\mathrm{SU}(2)_L\times\mathrm{U}(1)_Y$. However, a deeper understanding of the particle spectrum and its pattern of charge-changing weak transitions is still unknown.

One may try to understand the fermion spectrum and couplings by embedding the standard model in a larger gauge group. For example, unified theories of the electroweak and strong interactions based on the group SO(10) [1] can accommodate precisely this set of fermions within three 16-dimensional spinor representations. Larger unified groups, like E_6 [1–3], not only contain the standard model fermions but also predict the existence of new particles. The discovery of new particles predicted by higher dimensional gauge theories would provide insight into the organization of matter into a fundamental theory.

A unified theory based on the gauge group E_6 is phenomenologically interesting because it includes an enlarged lepton sector containing both massive and sterile neutrinos, an enlarged quark sector containing charge $-1/3$ isosinglet vectorlike quarks (ISVLQs), and additional gauge bosons (e.g. Z') [3,4]. The new quarks are vectorlike in the sense that their left-handed and right-handed chiralities have the same weak isospin (zero), in contrast to the usual *chiral* quarks which are left-handed doublets and right-handed singlets. A recent study of an E_6 grand unified model in which the lightest ISVLQ has a TeV scale mass (1.75 TeV) may be found in Ref. [5]. For information on building low-energy models from the gauge group E_6, consult Refs. [3,4,6–9].

In this paper, we study weak isosinglet vectorlike quarks with charge $-1/3$. Pair production of ISVLQs at high-energy hadron colliders is expected to be dominated by quantum chromodynamics (QCD) and thus to be precisely calculable. The decays of these particles depend on their mixing with SM down-type quarks [10–17]. We analyze the prospects for producing and detecting these exotic quarks at the Fermilab Tevatron and the CERN Large Hadron Collider (LHC). In particular, we consider both charged-current (mediated by $W^\pm$ bosons) and flavor-changing neutral-current (mediated by Z^0 and Higgs bosons) decays of the isosinglet vectorlike quark. The sensitivity of these estimates to assumptions about mixing between exotic quarks and those of the standard model is explored. A related study that investigates an extension of the standard model containing both singlet and doublet vectorlike quarks may be found in Ref. [18]. Earlier studies have appeared in Refs. [10,13].

The paper is organized as follows. In Sec. II, we review relevant properties of the exotic quarks, and we introduce a model for their mixing with ordinary quarks. In Sec. III, we briefly review constraints on the new mixing parameters. Based on these constraints, we propose a phenomenological parametrization of the Cabibbo-Kobayashi-Maskawa (CKM) matrix. Signals at the Fermilab Tevatron and the CERN LHC are treated in Secs. IV and V, respectively, while Sec. VI concludes.

II. THE MODEL

A. Matter states expected in E_6

In a unified electroweak theory based on the E_6 gauge group, the fundamental (27-dimensional) representation contains additional quarks with charge $-1/3$ and additional charged and neutral leptons. The exotic matter content of a single E_6 family is summarized in Table I [4]. We assume that there are three 27-plets, corresponding to the three lepton-quark families.

We adopt a ''bottom-up'' approach to a three-generation E_6 gauge field theory. Let M_1,M_2,M_3 denote the masses of the three exotic charge $-1/3$ quarks. For simplicity we assume that there is a mass hierarchy between the exotic quarks such that $M_1\ll M_2,M_3$. Hence, one of the exotic quarks will lie closer in the mass spectrum to the SM quark masses. In accordance with the literature [3,11,13], we de-

*Electronic mail: troy@hep.uchicago.edu
†Electronic mail: rosner@hep.uchicago.edu

TABLE I. Exotic fermions in a 27-plet of E_6.

SO(10)	SU(5)	State	Q	I_L	I_{3L}
10	5	h^c	1/3	0	0
		E^-	−1	1/2	−1/2
		ν_E	0	1/2	1/2
	5*	h	−1/3	0	0
		E^+	1	1/2	1/2
		$\overline{\nu_E}$	0	1/2	−1/2
1	1	n_e	0	0	0

note this exotic quark as h; one should not confuse the exotic h quark with the SM Higgs boson, denoted H^0. We assume h is the dominant exotic quark (relative to the two other exotic quarks) which mixes with the down-type SM quarks. Moreover, we assume that the exotic leptons (charged and neutral) do not significantly influence SM interactions or exotic-quark signatures at the center of mass (c.m.) energy of the Tevatron or the LHC. Production of exotic leptons, if kinematically allowed, should proceed only via the electroweak sector of the theory and thus should be suppressed with respect to exotic quark production. Under these assumptions, we have effectively reduced the E_6 model at the c.m. energies of the Tevatron and the LHC to a model that contains the SM along with a single down-type exotic quark.

The exotic quark h is a down-type quark, but unlike the SM quarks, the ISVLQ is a singlet under the $SU(2)_L$ factor of the SM gauge group. The singlet nature of the down-type ISVLQ introduces new mixings and interactions between the quarks. In the remainder of this section, we construct these interactions and explore their influence on the CKM matrix.

In this paper, the SM fermions are labeled by a generation index i ($i=1,2,3$) and we label the h quark by the index value 4. The indices (i,j,k) run from one to three and the indices (l,m,n) run from one to four. The "L" and "R" subscripts are employed to denote the left- and right-handed components of fermion fields (i.e., $u_{L,R}=P_{L,R}u=[\frac{1}{2}(1\mp\gamma^5)]u$ in our notation). To facilitate our discussion it is useful to define the left-handed quark doublet, and the left- and right- handed quark field vectors:

$$\mathcal{Q}_i=(u_{Li},d_{Li})^T,\quad U_A=(u_A,c_A,t_A)^T,$$

$$D_A=(d_A,s_A,b_A,h_A)^T, \tag{1}$$

where $A=L,R$. We denote the flavor eigenstates via the "0" superscript.

In the flavor basis, the kinetic piece of the quark Lagrangian is obtained via minimal coupling

$$\mathcal{L}_K=\overline{\mathcal{Q}_i^0}(i\not{\partial})\mathcal{Q}_i^0+\overline{h_L^0}(i\not{\partial})h_L^0+\overline{U_R^0}(i\not{\partial})U_R^0+\overline{D_R^0}(i\not{\partial})D_R^0$$
$$+gW_\mu^- J_{W^+}^\mu+gW_\mu^+ J_{W^-}^\mu+gZ_\mu^0 J_Z^\mu+eA_\mu J_{\text{e.m.}}^\mu, \tag{2}$$

where the $J_{\text{e.m.}}$, $J_{W^\pm}$, and J_Z are the electromagnetic, charged-weak, and neutral-weak current operators. In the weak eigenbasis these currents take the form

$$J_{W^+}^\mu=\frac{1}{\sqrt{2}}\sum_{i=1}^{3}[\overline{U_{Li}^0}\gamma^\mu D_{Li}^0],\quad J_{W^-}^\mu=\frac{1}{\sqrt{2}}\sum_{i=1}^{3}[\overline{D_{Li}^0}\gamma^\mu U_{Li}^0],$$

$$J_Z^\mu=\frac{1}{c_W}\Bigg\{C_L^u[\overline{U_L^0}\gamma^\mu U_L^0]+C_R^u[\overline{U_R^0}\gamma^\mu U_R^0]$$
$$+\sum_{i=1}^{3}C_L^d[\overline{D_{Li}^0}\gamma^\mu D_{Li}^0]$$
$$+C_R^d[\overline{D_R^0}\gamma^\mu D_R^0]+\frac{1}{3}s_W^2[\overline{h_L^0}\gamma^\mu h_L^0]\Bigg\},$$

$$J_{\text{e.m.}}^\mu=\frac{2}{3}[\overline{U_L^0}\gamma^\mu U_L^0+\overline{U_R^0}\gamma^\mu U_R^0]-\frac{1}{3}[\overline{D_L^0}\gamma^\mu D_L^0+\overline{D_R^0}\gamma^\mu D_R^0], \tag{3}$$

where s_W and c_W are the sine and cosine of the weak mixing angle, $C_L^a=I_L^a-Q_a s_W^2$ and $C_R^a=-Q_a s_W^2$ ($a=u,d$).

In the standard model, quark masses are generated when the Higgs doublet acquires a non-zero vacuum expectation value; the resulting mass terms in the Lagrangian have $\Delta I_L=1/2$. Unlike the SM, theories with exotic E_6 quarks have $\Delta I_L=0$ mass terms. In the ISVLQ model, these Dirac mass terms result from the left-handed h field [recall that h is an $SU(2)_L$ singlet] pairing with right-handed quark fields. We write the quark mass terms of the Lagrangian in the compact form

$$\mathcal{L}_{mass}=-\overline{U_L^0}\mathcal{M}^u U_R^0-\overline{D_L^0}\mathcal{M}^d D_R^0+\text{H.c.}, \tag{4}$$

where $\mathcal{M}^u$ and $\mathcal{M}^d$ are the up-type quark and down-type quark mass matrices, respectively. The up-type quark mass matrices mimic those of the SM; however, the down-type quark mass matrix has been enlarged. The down-type quark mass matrix contains both $\Delta I_L=1/2$ and $\Delta I_L=0$ entries.

It is important to distinguish the $\Delta I_L=1/2$ and $\Delta I_L=0$ mass terms since they may arise from fundamentally different scales. The $\Delta I_L=1/2$ mass terms are derived from spontaneous symmetry breaking of the SM Higgs boson at the electroweak scale; hence, these mass terms should be on the order of the electroweak scale or smaller. On the other hand, the $\Delta I_L=0$ mass terms do not result from electroweak symmetry breaking; therefore, they may be of any scale, possibly the unification scale. We distinguish $\Delta I_L=1/2$ and $\Delta I_L=0$ mass terms in the down-type quark matrix by lower- and upper-case letters, respectively,

$$\mathcal{M}^d=\begin{pmatrix} m_{dd} & m_{ds} & m_{db} & m_{dh} \\ m_{sd} & m_{ss} & m_{sb} & m_{sh} \\ m_{bd} & m_{bs} & m_{bb} & m_{bh} \\ M_{hd} & M_{hs} & M_{hb} & M_{hh} \end{pmatrix}. \tag{5}$$

We investigate the production and decay of an exotic E_6 quark at the Fermilab Tevatron and the CERN Large Hadron Collider. To understand exotic quark decay we must determine the branching ratios of these exotic fermions to SM particles. Hence we must determine the analogue of the

CKM matrix and the no longer trivial flavor-changing neutral current (FCNC) matrix for this theory, and we must constrain elements of these matrices by experimental data. To determine the CKM and FCNC matrices we must recast our theory in the *mass* eigenbasis.

Each quark mass matrix in this theory may be diagonalized by two unitary transformations, denoted L and R,

$$(\mathcal{M}^d)_{\rm diag}=(L^d)^\dagger \mathcal{M}^d R^d,\ \ (\mathcal{M}^u)_{\rm diag}=(L^u)^\dagger \mathcal{M}^u R^u \quad (6)$$

where the u and d unitary matrices are 3×3 and 4×4, respectively. The fields in the mass basis are related to the fields in the flavor basis by the L and R transformations:

$$D_L=(L^d)^\dagger D^0_{\rm L},\ D_R=(R^d)^\dagger D^0_{\rm R}, \quad (7)$$

$$U_L=(L^u)^\dagger U^0_{\rm L},\ \ U_R=(R^u)^\dagger U^0_{\rm R}.$$

Using the relations between the mass and flavor eigenstates, we recast the current operators of Eq. (3) in the mass eigenbasis:

$$J^\mu_{W^+}=\frac{1}{\sqrt{2}}V_{in}[\overline{U}_i\gamma^\mu {\rm P_L} D_n],\ \ J^\mu_{W^-}=\frac{1}{\sqrt{2}}V^*_{in}[\overline{D}_n\gamma^\mu {\rm P_L} U_i], \quad (8)$$

$$J^\mu_Z=\frac{1}{c_W}\{C^u_{\rm L}[\overline{U}_i\gamma^\mu {\rm P_L} U_i]+C^u_{\rm R}[\overline{U}_i\gamma^\mu {\rm P_R} U_i] + X_{nm}[\overline{D}_n\gamma^\mu {\rm P_L} D_m]+C^d_R[\overline{D}_n\gamma^\mu P_{\rm R} D_n]\},$$

$$J^\mu_{\rm e.m.}=\frac{2}{3}[\overline{U}_i\gamma^\mu U_i]-\frac{1}{3}[\overline{D}_n\gamma^\mu D_n],$$

where

$$V_{in}=\sum_{k=1}^{3}(L^u)^\dagger_{ik}L^d_{kn},\ \ X_{nm}=C^d_L\delta_{nm}+\frac{1}{2}L^{d*}_{4n}L^d_{4m} \quad (9)$$

denote the CKM and FCNC matrices ($i=1,2,3$, and $m,n=1,2,3,4$), respectively. One obtains the expression for the FCNC matrix by transforming the coupling of the left-handed down-type quarks to the Z^0 from the weak basis to the mass basis,

$$\mathcal{L}\supset\frac{g}{c_W}Z^0_\mu\left[\overline{D}^0_{{\rm L},m}\gamma^\mu\left(C^d_{\rm L}\delta_{mn}+\frac{1}{2}\delta_{4m}\delta_{4n}\right)D^0_{{\rm L},n}\right]$$

$$\supset\frac{g}{c_W}Z^0_\mu\left[\overline{D}_{{\rm L},m'}\gamma^\mu L^{d*}_{m'm}\left(C^d_{\rm L}\delta_{mn}+\frac{1}{2}\delta_{4n}\delta_{4m}\right)L^d_{nn'}D_{{\rm L},n'}\right]$$

$$\supset\frac{g}{c_W}Z^0_\mu\left[\overline{D}_{m'}\left(C^d_{\rm L}\delta_{m'n'}+\frac{1}{2}L^{d*}_{4n'}L^d_{4m'}\right)\gamma^\mu {\rm P_L} D_{n'}\right]. \quad (10)$$

Note: If the ISVLQ were an up-type quark, then the Z^0 boson would have a corresponding FCNC coupling to the up-type quarks of the form $C^u_{\rm L}\delta_{mn}-\frac{1}{2}L^{u*}_{4n}L^u_{4m}$.

This theory differs from the SM in the structures of its CKM and FCNC matrices. In the SM, the CKM matrix is a 3×3 *unitary* matrix, while in the ISVLQ model it is a 3×4 matrix (non-unitary). Hence the ''unitarity triangle'' approach to determining CKM parameters must be abandoned in favor of a ''unitarity quadrangle'' [19]. In the SM, the FCNC matrix is diagonal; hence, there are no tree-level flavor-changing neutral couplings. In the ISVLQ model this is no longer true; in essence, one abandons the Glashow-Iliopoulos-Maiani (GIM) mechanism [20] which suppresses flavor-changing neutral currents. In Sec. III, we investigate the structure of the CKM and FCNC matrices (both matrices are related to the L^d matrix).

B. Feynman Rules

As explained in Sec. II A, we consider a simple E_6 inspired extension of the SM, in which one down-type ISVLQ interacts with the SM particles. In Fig. 1, we summarize the effects of this ISVLQ on the quark interactions with SM gauge and scalar fields. In this paper, all calculations are performed in the Feynman–'t Hooft gauge.

The addition of an ISVLQ not only induces Z^0-mediated tree-level FCNC interactions, but also induces tree-level FCNCs mediated by the Higgs, H^0, and Goldstone, ϕ^Z, bosons. Therefore, in certain instances, the branching ratio of the h quark to a Higgs boson is large.

III. CONSTRAINTS AND THE PARAMETRIZATION OF THE CKM MATRIX

A. Physical parameters

It is useful to parametrize the complex non-unitary 3×4 CKM matrix in terms of physical parameters. The number of physical parameters of a theory may be determined by analyzing its symmetries. Consider the up- and down-type quark mass matrices in Eq. (4); each mass matrix is complex, hence there are $(9+16)\times2=50$ real parameters. To determine the number of physical parameters let us *turn off* the mass matrices. Setting the quark mass matrices to zero, the theory admits a global quark symmetry,

$$\mathcal{G}_{Global}(\mathcal{M}^u=\mathcal{M}^d=0)={\rm U}(3)_Q\times{\rm U}(4)_{\overline{d}}\times{\rm U}(3)_{\overline{u}}\times{\rm U}(1)_h, \quad (11)$$

where the subscripts Q, $\overline{d}$, $\overline{u}$, and h correspond to the left-handed SM quarks [transforming as 2 under $SU(2)_{\rm L}$], right-handed down-type quarks, right-handed up-type quarks, and left-handed ISVLQ, respectively. This global symmetry contains $9+16+9+1=35$ real parameters. If we turn the quark mass matrices back on, then the global symmetry is spoiled and we are left with a remnant global U(1) quark symmetry. Consequently, there are $50-35+1=16$ *physically* significant real parameters: 7 quark masses, and 9 mixing parameters (6 angles and 3 phases). One uses the 9 physical mixing parameters to parametrize the unitary matrices of the theory (L^d,R^d,L^u, and R^u) and hence the CKM and FCNC matrices.

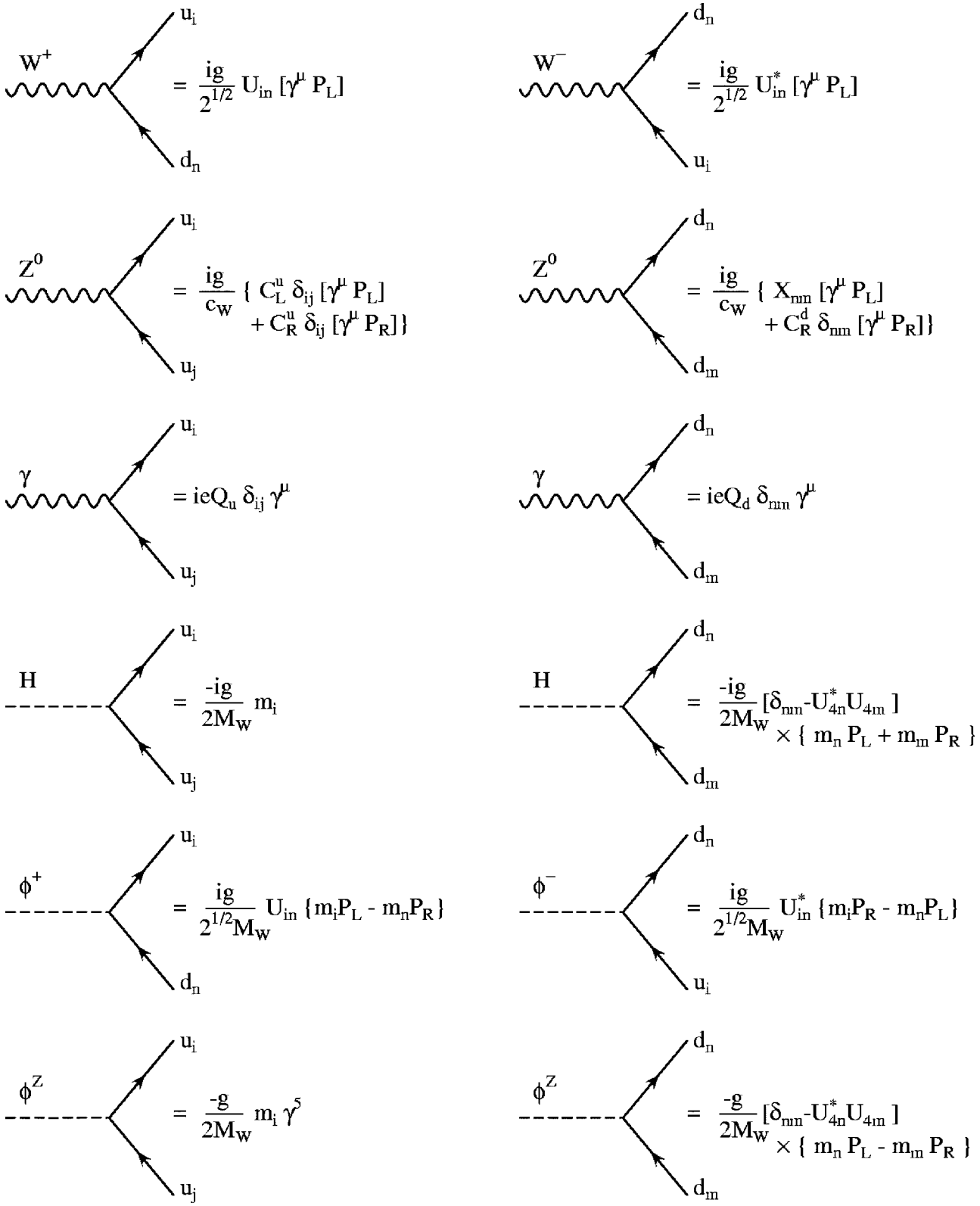

FIG. 1. Feynman rules for a model with one ISVLQ down quark. The indices $i,j = 1,2,3$ and the indices $n,m = 1,2,3,4$.

Assuming that we have solved for the up-type quark mass eigenstates, then the CKM matrix expression (9) reduces to

$$V_{in}=L^{d}{}_{in}, \tag{12}$$

where $i=1,2,3$ and $n=1,2,3,4$. If we parametrize the 4×4 *unitary* L^d matrix, we recover the CKM matrix by restrictingto the upper 3×4 sub-matrix. We recover the FCNC matrix by selecting appropriate combinations of the L^d_{4m} entries [see Eq. (9)].

B. Constraints on *h* quark mixings

The L^d matrix may be parametrized by nine physical parameters; however, the ISVLQ model does not specify the magnitude and pattern of the resulting interactions. Because we are interested in the production and decay of *h* quarks, constraints on the magnitude of the new mixings between the *h* quark and the SM quarks are important. To determine the magnitude and pattern of these and other interactions (charged-current and flavor-changing neutral-current), experimental data must be examined. Using experimental constraints on elements of the CKM and FCNC matrices, one may infer the structure of the L^d matrix [consult Eq. (9)].

Data from precision electroweak experiments and low-energy flavor-changing neutral processes help to constrain CKM and FCNC matrix elements. We use recent constraints on CKM and FCNC matrix elements obtained by Refs. [21,22]. For additional information on constraints of the CKM and FCNC matrix elements in an ISVLQ model, we refer the reader to studies discussed in Refs. [11,13,15,19,23,24]. In Ref. [21], the following constraints on the magnitudes of L^d matrix elements were obtained: $0\leqslant|L^d_{14}|\leqslant0.087$, $0\leqslant|L^d_{24}|\leqslant0.035$, $0\leqslant|L^d_{34}|\leqslant0.041$, and $0.998\leqslant|L^d_{33}|\leqslant1$.

The constraint on the magnitude of L^d_{33} is required by the agreement of R_b with experiment. Constraints on the magnitude of the L^d_{i4} $(i=1,2,3)$ matrix elements are obtained from observables that depend on the product of L^d matrix elements (e.g. $L^{d*}_{14}L^d_{24}$). Measurements of $|\Delta m_K|$ and the branching ratios $K^+\rightarrow\pi^+\nu\bar{\nu}$ and $K_L\rightarrow\mu^+\mu^-$ constrain the product $L^{d*}_{42}L^d_{41}$; a measurement of ϵ'/ϵ constrains $\mathrm{Im}(L^{d*}_{42}L^d_{41})$. The product $L^{d*}_{41}L^d_{43}$ is constrained by $|\Delta m_B|$ and the *CP* asymmetry $a_{\psi K_s}$. $L^{d*}_{42}L^d_{43}$ is constrained by $|\Delta m_{B_s}|$ and the branching ratios $b\rightarrow se^+e^-$, $b\rightarrow s\mu^+\mu^-$. Reference [21] also finds that, at present, there are no restrictions on *h* quark masses below 1 TeV/c^2. Using the constraints on the L^d matrix in addition to constraints on the mixing between SM quarks, we can parametrize the L^d matrix.

C. Wolfenstein parametrization

There are a number of ways to parametrize the L^d matrix, and hence the CKM matrix. We adopt a Wolfenstein-inspired [25] parametrization. We require the elements of the principal diagonal and the sub-diagonal directly above the principal diagonal to be real. In analogy with the phase in the SM Wolfenstein parametrization, the two new phases of the matrix are assigned to the L^d_{14} and L^d_{24} elements. The presence of additional phases in the ISVLQ model may lead to additional sources of *CP* violation; for studies of *CP* violation arising from the new phases of the L^d matrix the reader should consult Refs. [26–29].

We write $L^d_{14}=A\nu e^{i\omega_2}\lambda^{2+n_{14}}$, and $L^d_{24}=A\kappa e^{i\omega_2}\lambda^{2+n_{24}}$, where ω_2 and ω_3 are the two new phases, ν and κ [$\nu,\kappa\sim\mathcal{O}(1)$] are two of the three new angles, the Wolfenstein "*A*" parameter is inserted for convenience, and n_{14} and n_{24} are integers greater than or equal to 0. If the *h* quark were to mix strongly with either the *u* or *c* quarks [i.e., if L^d_{14} or L^d_{24} were of $\mathcal{O}(\lambda)$], then current SM mixing contained in the first two rows of the L^d and CKM matrix would be affected [30]. The third new angle, ξ, parametrizes the mixing of the ISVLQ with the third generation of quarks. We parametrize the L^d_{34} matrix elements as $\xi\lambda^2$ where $\xi\sim\mathcal{O}(1)$. The magnitudes of the L^d_{14}, L^d_{24}, and L^d_{34} elements are consistent with the constraints on the L^d matrix outlined in Sec. III B ($\xi\leqslant1$ from bound on L^d_{34}).

Using this framework, we create a preliminary sketch of the L^d matrix:

$$L^d=\begin{pmatrix} 1-\frac{1}{2}\lambda^2+l_{ud} & \lambda & A\mu e^{i\omega_1}\lambda^3 & A\nu e^{i\omega_2}\lambda^{2+n_{14}} \\ -\lambda+l_{cd} & 1-\frac{1}{2}\lambda^2+l_{cs} & A\lambda^2 & A\kappa e^{i\omega_3}\lambda^{2+n_{24}} \\ c_{td}\lambda^3+l_{td} & c_{ts}\lambda^2+l_{ts} & 1-c_{tb}\lambda^4+l_{tb} & \xi\lambda^2 \\ L^d_{41} & L^d_{42} & L^d_{43} & 1-c_{4h}\lambda^4+l_{4b} \end{pmatrix}, \tag{13}$$

where the c_{nm} are multiplicative factors of $\mathcal{O}(1)$, and the l_{nm} are *higher-order* contributions in λ to the L^d_{nm} elements [e.g. in the L^d_{32} element, $l_{ts}\sim\mathcal{O}(\lambda^3)$ since $c_{ts}\lambda^2$ is of second order in λ]. Using the unitarity of the L^d matrix and additional assumptions regarding the size of particular elements, one may obtain a fully parametrized expression for the L^d matrix.

As previously mentioned, we expect the *h* quark to mix predominantly with the third generation. Therefore, to simplify the parameter space we assume that the mixing of the *h* quark with the first two generations is small; namely, we assume that n_{14} and n_{24} are greater than the order of the L^d matrix parametrization. Parametrizing L^d to $\mathcal{O}(\lambda^5)$, one obtains the following matrix:

$$L^d = \begin{pmatrix} 1-\frac{1}{2}\lambda^2-\frac{1}{8}\lambda^4 & \lambda & A\mu e^{i\omega_1}\lambda^3 & 0 \\ -\lambda & 1-\frac{1}{2}\lambda^2-(\frac{1}{8}+\frac{1}{2}A^2)\lambda^4 & A\lambda^2 & 0 \\ A(1-\mu e^{-i\omega_1})\lambda^3 & -A\lambda^2-A(-\frac{1}{2}+\mu e^{-i\omega_1})\lambda^4 & 1-(\frac{1}{2}\xi^2+\frac{1}{2}A^2)\lambda^4 & \xi\lambda^2 \\ 0 & A\xi\lambda^4 & -\xi\lambda^2 & 1-\frac{1}{2}\xi^2\lambda^4 \end{pmatrix}. \quad (14)$$

In this parametrization of the L^d matrix, the phase $\omega_1 = -\gamma$ and the angle $\mu = \sqrt{\rho^2+\eta^2}$.

Using this form of the L^d matrix and Eq. (9), the dominant *new* charged-current coupling is between the top and h quarks. The strength of the t-h charged-current interaction is $g(2^{-1/2})\xi\lambda^2$. In the ISVLQ model, tree-level FCNCs are expected between all four down-type quarks; however, we find that tree-level flavor-changing neutral currents between SM quarks are disfavored [$\mathcal{O}(\lambda^6)$]. Interactions between the h quark and SM down-type quarks may be sizable; in fact, interactions between the h quark and b and s quarks are of $\mathcal{O}(\lambda^2)$ and $\mathcal{O}(\lambda^4)$, respectively. In particular, the h-b interaction is *left handed* with strength $g(2c_W)^{-1}\xi\lambda^2$ [to $\mathcal{O}(\lambda^5)$ in the parametrization].

The form of the L^d matrix in Eq. (14) is just one of many possibilities arising from the constraints in Sec. III B. For example, the strength of the charged-current interaction between the h quark and the u or c quarks may not be negligible (e.g. n_{14} or n_{24} may equal zero). If these charged-current interactions are relevant, then they will contribute to the "td" and "ts" elements of the CKM matrix. These additional charged-current interactions lead to corrections to the l_{td} and l_{ts} terms of the L^d_{31} and L^d_{32} elements. In the remainder of this paper, we use the L^d matrix in Eq. (14).

IV. $h\bar{h}$ PRODUCTION AND DECAY SIGNATURES AT THE FERMILAB TEVATRON

In this section we investigate the prospects for h quark observation at the Fermilab Tevatron. In $p\bar{p}$ and pp collisions, $h\bar{h}$ production proceeds predominantly through QCD interactions; therefore, in the remainder of our analysis, we suppress contributions to $h\bar{h}$ production from electroweak processes.

A. $h\bar{h}$ production

To obtain a basic understanding of the $h\bar{h}$ production rate and the h quark mass reached at hadron colliders, we plot (see Fig. 2) the tree-level $h\bar{h}$ pair production cross section at the Fermilab Tevatron ($\sqrt{s}=1.96$ TeV) and CERN LHC ($\sqrt{s}=14$ TeV) as a function of the h quark mass, calculated using the CTEQ5L structure functions [31]. The curves in each of these plots correspond to different choices of the QCD Q scales [$Q^2=M_Z^2$, m_h^2, $(2m_h)^2$, and $\hat{s}$]. For small h quark masses the cross sections for each of the Q scales are comparable; however, at h quark masses above ~ 200 GeV/c^2 there is a large discrepancy between the cross section with the fixed Q scale ($Q^2=M_Z^2$) and the dynamic Q scale [$Q^2=m_h^2$, $(2m_h)^2$, and $\hat{s}$]. For our analysis at the Tevatron we use a Q scale which is set by the c.m. energy of the subprocess, and at the LHC we use a Q scale equal to twice the h quark mass.

Using Fig. 2 and projected integrated luminosities, a "back of the envelope" upper limit for the h quark mass reach is obtained. For an integrated luminosity of

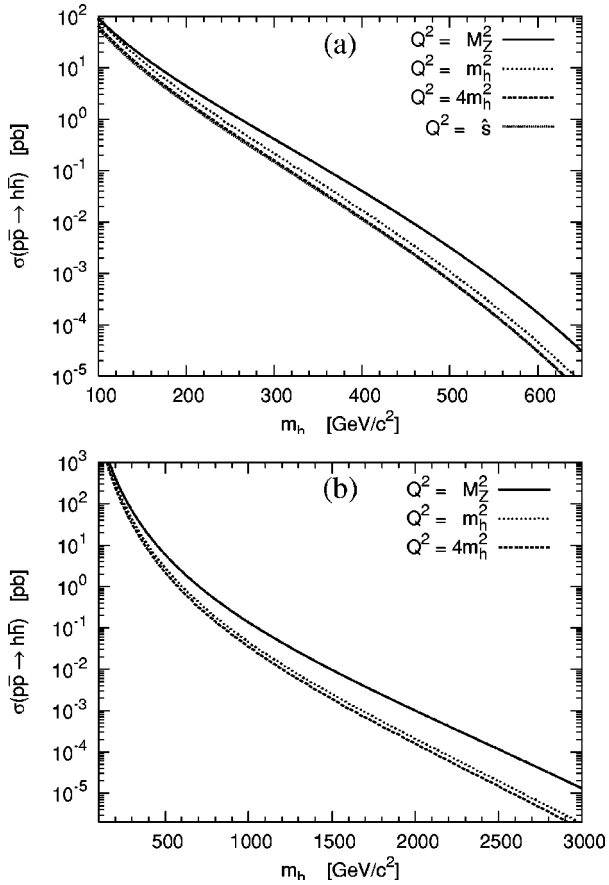

FIG. 2. Plot of the $h\bar{h}$ production cross section as a function of the h quark mass at (a) the Fermilab Tevatron, $\sqrt{s}=1.96$ TeV, and at (b) the CERN LHC, $\sqrt{s}=14$ TeV. The curves in each of these plots correspond to different choices of the QCD scale [$Q^2=M_Z^2$, m_h^2, $(2m_h)^2$, and $\hat{s}$], where $\hat{s}$ is the square of the subprocess c.m. energy. In the Tevatron plot, the curves for $Q^2=(2m_h)^2$ and $Q^2=\hat{s}$ overlap, while in the LHC plot we omit the $Q^2=\hat{s}$ curve since the CTEQ5L structure functions [31] are not defined beyond 10 TeV.

(1, 10) fb^{-1} at the Tevatron, the largest h quark mass reachable (producing at least one $h\bar{h}$ event) is $\sim$(490, 550) GeV/c^2. At a luminosity of 100 fb^{-1} at the LHC, the largest accessible h quark mass reachable is $\sim$2500 GeV/c^2. These estimates assume perfect event detection and they assume there are no complications arising from the decay of the h quarks.

Though Fig. 2 is instructive, one must take into consideration final-state signatures and backgrounds to determine a realistic h quark mass reach. The h quark is expected to be an unstable particle and hence it will decay to SM particles. The three dominant h quark decay processes are $h\to tW^-$, $h\to bZ^0$, and $h\to bH^0$. Since each decay mode of the h quark depends on the new mixing parameter ξ, the cross section for h quark production and decay must also depend on the mixing parameter.

We calculate the cross sections for $h\bar{h}$ pair production in conjunction with decay of the h quark into a SM quarks and gauge bosons. To facilitate this analysis we use the COMPHEP [32] software package to calculate the tree-level cross sections for $h\bar{h}$ production and decay at the two collider facilities. For the remainder of this section we shall restrict our analysis to the Fermilab Tevatron, reserving a brief discussion of the LHC for Sec. V.

B. h quark width

To calculate the cross sections for $h\bar{h}$ production and subsequent decay, we must first calculate the width of the h quark. The total width of the h quark is the sum of the h quark partial widths; the decay processes contributing to the partial widths may be separated into three (decay) channels: $h\to u_iW^-$, $h\to d_iZ^0$, and $h\to d_iH^0$. To leading order the partial widths for the three decay channels are given by the expressions

$$\Gamma(h\to u_iW^-)=\left(\frac{G_F}{4\sqrt{2}\pi}\right)\left(\frac{c_W^2M_Z^2}{m_h^2}\right)|L_{i4}|^2 \times p^*(m_h,m_i,c_W^2M_Z)F(m_h^2,m_i^2,c_W^2M_Z^2),$$

$$\Gamma(h\to d_iZ^0)=\left(\frac{G_F}{8\sqrt{2}\pi}\right)\left(\frac{M_Z^2}{m_h^2}\right)|L_{4i}^d|^2|L_{44}^d|^2 \times p^*(m_h,m_i,M_Z)F(m_h^2,m_i^2,M_Z^2),$$

$$\Gamma(h\to d_iH^0)=\left(\frac{G_F}{8\sqrt{2}\pi}\right)\left(\frac{c_W^2M_Z^2}{m_h^2}\right)|L_{4i}^d|^2|L_{44}^d|^2 \times p^*(m_h,m_i,\mathrm{M_H})G(m_h^2,m_i^2,\mathrm{M_H^2}), \quad (15)$$

where p^* is the center of mass momentum, and

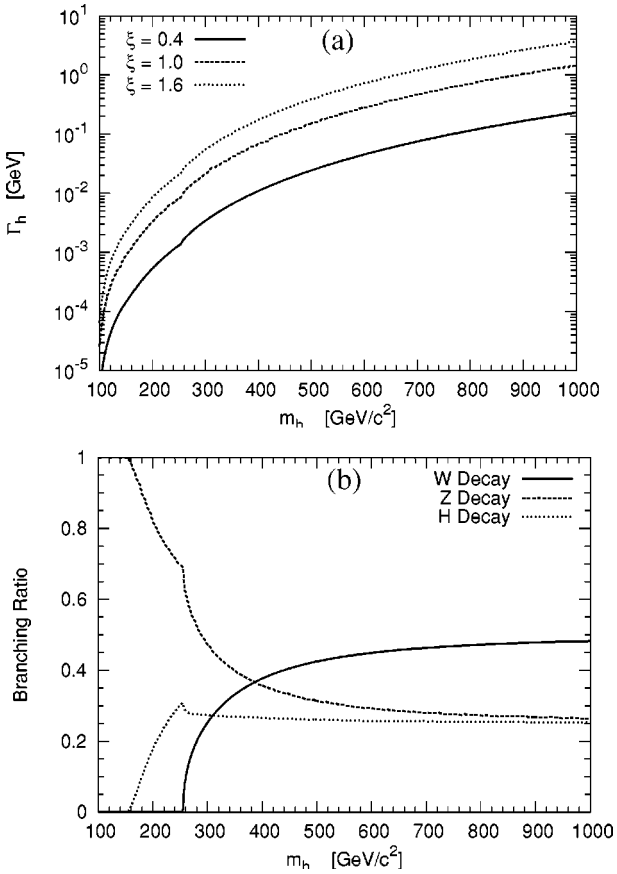

FIG. 3. (a) Plot of the h quark partial widths as a function of the mixing parameter ξ ($=0.4,1.0,1.6$) and h quark mass, m_h. (b) Plot of the h quark branching ratio for a fixed mixing parameter value $\xi=1$ and a variable h quark mass, m_h. In each of these plots, the Higgs boson mass is taken to be 150 GeV/c^2.

$$F(m_1^2,m_2^2,M^2)=m_1^2+m_2^2-M^2+\frac{1}{M^2}(m_1^2-m_2^2-M^2)\times(m_1^2-m_2^2+M^2),$$

$$G(m_1^2,m_2^2,M^2)=\frac{1}{c_W^2M_Z^2}[4m_1^2m_2^2+(m_1^2+m_2^2)(m_1^2+m_2^2-M^2)]. \quad (16)$$

The center of mass momentum may be expressed as $p^*(m_1,m_2,M)=(1/2m_1)[\lambda(m_1^2,m_2^2,M^2)]^{1/2}$, where $\lambda(a,b,c)=a^2+b^2+c^2-2ab-2ac-2bc$. The partial widths for h quark decays (via the W^-, Z^0 and H^0 channels) are shown in Fig. 3(a).

In Fig. 3(b), we plot the branching ratio for the h quark decaying via Z^0, W^-, and H^0 channels. In this plot the mixing parameter, ξ, is 1, the mass of the Higgs boson is 150 GeV/c^2, and the mass of the h quark is varied from 100 to 1000 GeV/c^2. The Z^0 decay mode is the dominant decay channel for h quark masses below 200 GeV/c^2; however, the branching ratio to this mode quickly diminishes as the H^0

and $W^{\pm}$ decay modes become kinematically accessible. Since the charged-current u and c couplings to the h quark are small [see Eq. (14)], the branching ratio of the h quark to W^- is suppressed until $m_h \geq M_W + m_t$. In the large h quark mass limit, the ratios of the Z^0, H^0, and W^- partial widths are $|L^d_{44}|^2 : |L^d_{44}|^2 : 2$. Using the L^d matrix parametrization in Eq. (14), these ratios are $(1-\xi^2\lambda^4) : (1-\xi^2\lambda^4) : 2$.

C. Constraints on ISVLQ model from b' searches

Before we discuss specific signatures of $h\bar{h}$ pair production and their corresponding cross sections, we investigate limits on the h quark mass from previous experiments. In particular, we determine implied limits from the first run of the Fermilab Tevatron.

In run IB of the Fermilab Tevatron ($\sqrt{s} = 1.8$ TeV), the CDF and DØ Collaborations acquired 86.47 pb^{-1} and 84.5 pb^{-1} of data, respectively [33]. Although a specific analysis of the ISVLQ model using the run IB data was not considered, we can infer limits on the h quark mass from b' searches [34–36]. Unlike the ISVLQ h quark, the b' is the charge $-1/3$ member of a fourth quark generation, $(t'\ b')^{\mathrm{T}}$. Since the b' is a member of a doublet, the GIM mechanism is preserved and, therefore, flavor-changing neutral decays of the b' are forbidden at tree level. Consequently, flavor-changing b' decays occur via higher-order interactions; they are expected to be suppressed relative to tree-level interactions.

In these b' studies, the CDF and DØ Collaborations searched for a fourth-generation b' quark by looking for events where the b' decays via a flavor-changing neutral interaction. In particular, both the CDF and the DØ Collaborations searched for a b' quark in the following mass regions: (1) $m_{b'} < M_Z$ (see Ref. [34]) and (2) $m_{b'} > M_Z + m_b$ but $m_{b'} < m_t$ and $m_{b'} < m_{t'}$ (see Ref. [35]). In the former mass region, the b' decays to a photon and a SM down-type quark, while in the latter mass region the b' decays predominantly to a Z^0 boson and a SM down-type quark. Note that in the second mass region, tree-level charged-current decays to light, up-type quarks are present; however, they are doubly Cabibbo suppressed by the small coupling between the b' quark and the light up-type quarks.

In this paper, we are interested in an ISVLQ h quark with a mass greater than that of the Z^0 boson. In the top panel of Fig. 4, we reproduce the 95% confidence limit (solid line) on the cross section for a b' quark of Ref. [35]. In the bottom panel of Fig. 4, we plot the cross section for the $h\bar{h}$ production multiplied by the branching ratio for each h quark to the Z^0 mode. The four curves in this plot correspond to the aforementioned choices of the QCD Q scale. Using the $\sqrt{\hat{s}}\ Q$ scale, one finds that for a mixing parameter of $\xi = 1$ and a Higgs boson mass of 150 GeV/c^2 the run I data exclude an h quark at the 95% confidence level in the 100–200 GeV/c^2 mass range. For a Higgs boson mass of 115 GeV/c^2, the run I analyses imply that an h quark is excluded in the mass range of 100–185 GeV/c^2. In the following sections, we will discuss the effect of the ξ mixing parameter on the h quark mass reach of current and future hadron colliders.

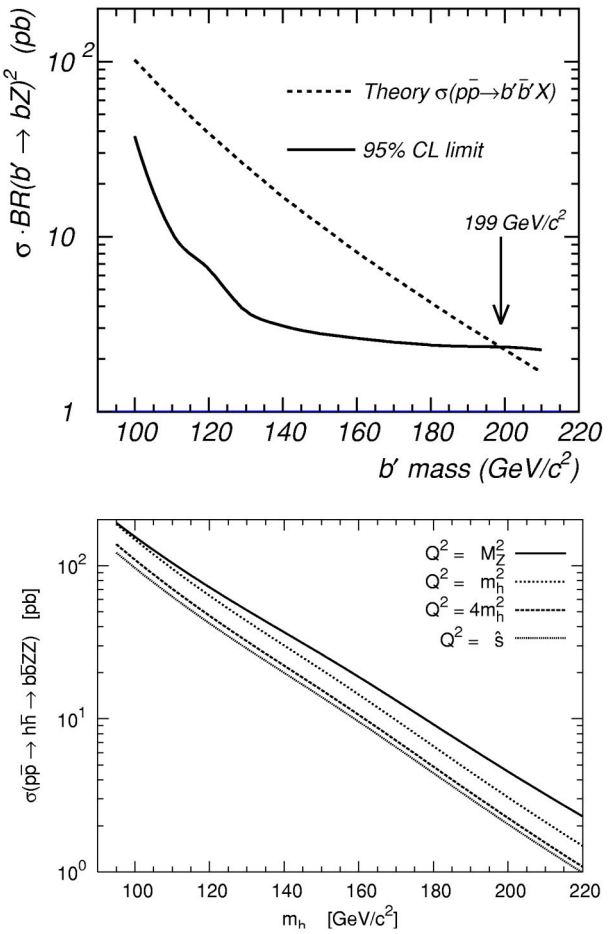

FIG. 4. (Top) Exclusion plot for the b' search from run IB of CDF [35]. (Bottom) Plot of the cross section for h quark pair production and subsequent decay into two b quarks and two Z^0 bosons. In this plot the mixing parameter $\xi = 1$, the Higgs boson mass is 150 GeV/c^2, and the curves correspond to different values of the Q^2 scale.

D. $h\bar{h}$ production and decay at the Tevatron

At the c.m. energy of the Fermilab Tevatron ($\sqrt{s} = 1.96$ TeV), $h\bar{h}$ pair production is dominated by subprocesses in which a quark from a proton and an anti-quark from an anti-proton annihilate via a strong interaction. Contributions from subprocesses involved in gluon-gluon fusion are suppressed by the gluon density of the proton, and sea quark contributions are suppressed by the sea quark distributions of the proton.

Once an $h\bar{h}$ pair is produced, each isosinglet quark decays to a SM quark and an associated gauge or scalar boson. Although subsequent decay and hadronization of these particles is expected, we do not explicitly generate the matrix elements for these individual processes. Rather, we generate the matrix elements for $h\bar{h}$ pair production and the primary decay of the h quarks into a heavy quark (bottom or top) and an associated gauge or scalar boson. We *do not* consider processes in which the primary decay of the h quark results in a light quark. Processes in which the h quark decays to a W^- and a light quark are disfavored by our choice of CKM

TABLE II. We require that the h quark decay products pass basic pseudorapidity (η), transverse momentum (p_T), and angular separation (ΔR) cuts. Note that the angular separation cut is applied only to the bottom quarks and not to the top quark or the bosons (gauge nor scalar).

Parameter	Minimum value	Maximum value
η_b	-3.0	3.0
$\Delta R(b_1,b_2)$	0.4	–
p_T^b	25.0	–

matrix [see Eq. (14)]; moreover, processes in which the h quark decays to a Z^0 or an H^0 and a light down-type quark often lead to complicated, multi-jet event topologies.

For the Tevatron, the $h\bar{h}$ production and decay schemes considered in this paper are as follows:

1. $p\bar{p} \rightarrow h\bar{h} \rightarrow t\bar{t}W^+W^-$,
2. $p\bar{p} \rightarrow h\bar{h} \rightarrow b\bar{b}Z^0Z^0$,
3. $p\bar{p} \rightarrow h\bar{h} \rightarrow b\bar{b}H^0H^0$,
4. $p\bar{p} \rightarrow h\bar{h} \rightarrow b\bar{b}H^0Z^0$,
5. $p\bar{p} \rightarrow h\bar{h} \rightarrow t\bar{b}W^-Z^0+\bar{t}bW^+Z^0$,
6. $p\bar{p} \rightarrow h\bar{h} \rightarrow t\bar{b}W^-H^0+\bar{t}bW^-H^0$.

Promising final-state signatures and backgrounds for these processes are discussed in Secs. IV D 1 and IV D 2, respectively. For the time being, we are interested in the cross sections for these six $h\bar{h}$ production/decay schemes and which, if any, of these schemes provides the best channel(s) for an h quark search at the Tevatron.

To begin, we impose a loose set of cuts to ensure that the $h\bar{h}$ events produced conform to *basic* geometry and event selection requirements of the detectors. These cuts are summarized in Table II. We impose a loose cut on the pseudorapidity η of the bottom quark, $|\eta_b|<3$. Pseudorapidity is defined as $\eta=-\log\tan(\theta/2)$, where θ is the angle between the particle being considered and the undeflected beam. In addition to the pseudorapidity cut, we impose a jet separation cut, $\Delta R=\sqrt{(\Delta\eta)^2+(\Delta\phi)^2}$, to ensure that there is adequate jet separation for detection. Finally, we impose a cut on the transverse momentum, p_T, of the bottom quark. Because the bottom quark is a decay product of a much heavier h quark, one expects the bottom quarks to be ''hard'' (high momentum) and to have substantial transverse momentum which scales with the mass of the h quark. Moreover, because previous data from the Fermilab Tevatron appear to exclude an h quark up to $\sim$200 GeV/c^2 (when $M_H=150$ GeV/c^2), a ''hard'' cut on the transverse momentum of the b quark will merely reduce the h quark signal in a previously excluded region (i.e. 100–200 GeV/c^2). Therefore, we impose a lower bound of 25 GeV/c on the transverse momentum of each b quark. As we shall discuss in Sec. IV D 2, the p_T cut and the ΔR cut on the b quarks help to reduce backgrounds for these $h\bar{h}$ pair production processes. The top quark and the gauge bosons are unstable particles; therefore, we do not impose any constraints on these particles. When we discuss

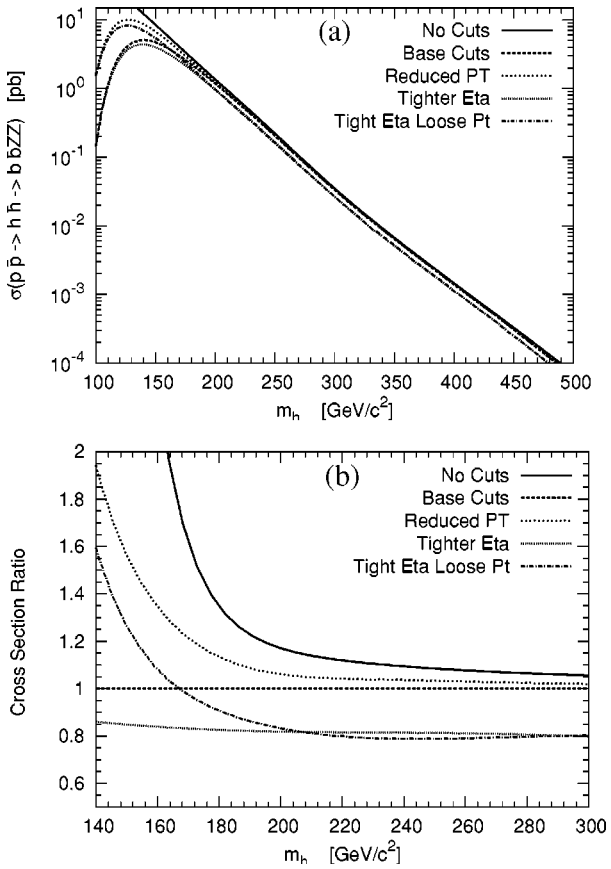

FIG. 5. Effect of cuts on the $p\bar{p}\rightarrow h\bar{h}\rightarrow b\bar{b}Z^0Z^0$ cross section where the mixing parameter $\xi=1$, and the Higgs boson mass $M_H=150$ GeV/c^2. (a) Plot of $\sigma(p\bar{p}\rightarrow h\bar{h}\rightarrow b\bar{b}Z^0Z^0)$ for five different choices of b quark cuts: (solid) *No Cuts*; (long dash) *Base Cuts*, see Table II; (short dash) *Reduced* p_T, base cuts with $p_T^b>15$ GeV/c; (dots) *Tighter* η, base cuts with $|\eta_b|<1.5$; (dash-dot) *Tight* η and *Loose* p_T, base cuts with the tighter η and a looser p_T. (b) Plot of the cross sections relative to the ''Base Cuts'' cross section.

event signatures in Sec. IV D 1, we will impose cuts on the decay products of these particles.

In Fig. 5, we illustrate the effects of these cuts on the $p\bar{p}\rightarrow h\bar{h}\rightarrow b\bar{b}Z^0Z^0$ signal. In Fig. 5(a), we plot the $p\bar{p}\rightarrow h\bar{h}\rightarrow b\bar{b}Z^0Z^0$ cross section for the following cuts: ''no cuts'' (unconstrained), ''base cuts'' (see Table II), ''tighter η'' cut ($|\eta_b|<1.5$), ''reduced p_T'' cut ($p_T^b>15$ GeV/c), and ''tight η/loose p_T'' cut ($|\eta_b|<1.5$ and $p_T^b>15$ GeV/c). In Fig. 5(b), we present each of these cross sections divided by the ''base cuts'' cross section. Above an h quark mass of 180 GeV/c^2, loosening the transverse momentum cut from 25 GeV/c to 15 GeV/c on each b quark increases the cross section by less than 10%. Tightening the pseudorapidity cut from 3 to 1.5 on *both* b quarks reduces the cross section by roughly 20%. Modified constraints on the b quark pseudorapidity may be used to limit the reduction in the cross section to less than 20%. For example, one may require at least one b quark to be ''tight'' ($\eta_b<1.5$) and the other b quark to be ''loose'' ($\eta_b<3$).

The cross sections for $h\bar{h}$ production and (primary h quark) decay are shown in Fig. 6. The new mixing parameter

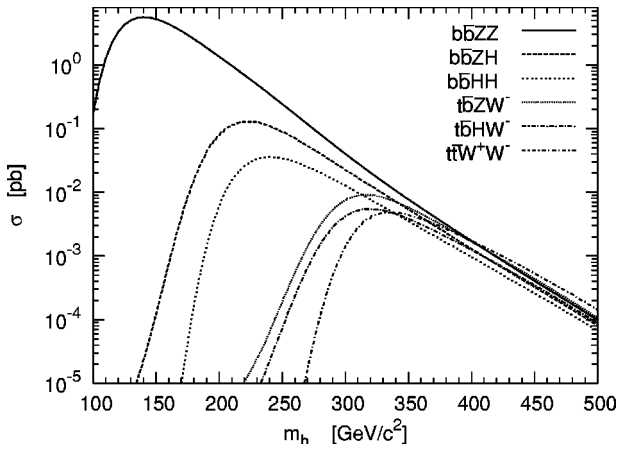

FIG. 6. Cross sections for $h\bar{h}$ production and primary decay at the Fermilab Tevatron. In this plot the Higgs boson mass is $M_H = 150$ GeV/c^2, $\xi = 1$, and $Q = \sqrt{\hat{s}}$.

ξ is set to 1 and the h quark mass, m_h, runs from 100 to 500 GeV/c^2. The cross sections for each of the primary decay modes fall rapidly as the h quark mass is increased. Because of the transverse momentum cut on the b quarks, primary decay modes containing at least one b quark exhibit exaggerated rounding of peaks in the cross section. Cross sections for modes in which the decay products of the h quark are more massive than the h quark are suppressed. In particular, the cross section for the $t\bar{t}W^+W^-$ mode is suppressed until $m_h \geq m_t + M_W$. As a result of the suppression and the c.m. energy of the Tevatron, cross sections for modes in which at least one h quark decays to a top quark are small (less than 10 fb).

At an integrated luminosity of (1, 10) fb^{-1}, the largest accessible h quark mass (at $\xi = 1$ and $M_H = 150$ GeV/c^2) for any of the primary h decay modes is $\sim$(420, 500) GeV/c^2 (modes produce one signal event). The most promising of these primary decay modes are the $b\bar{b}Z^0Z^0$ and $b\bar{b}H^0Z^0$ modes. Each of these modes has a "large" cross section below an h quark mass of 300 GeV/c^2, and their respective cross sections are comparable to the other modes above an h quark mass of 300 GeV/c^2. As discussed in Sec. IV D 1, these modes can give rise to clean distinctive signatures at the Tevatron. On the other hand, modes in which at least one h quark decays to the tW^- channel have relatively small cross sections at the Tevatron. Subsequent decay of the top quark often leads to complicated final states.

Effect of the ξ mixing parameter on cross sections. Before we discuss signatures of $h\bar{h}$ pair production at the Tevatron, we address the dependence of the cross sections on the mixing parameter, ξ, and on the Higgs mass. In Fig. 7(a) and Fig. 7(c), we plot the $p\bar{p} \to h\bar{h} \to b\bar{b}Z^0Z^0$ and $p\bar{p} \to h\bar{h} \to b\bar{b}H^0Z^0$ cross sections for a Higgs boson mass of 150 GeV/c^2 and for four choices of the ξ parameter, $\xi = 0.02$, 0.2, 1, 2 [37]. In Fig. 7(b) and Fig. 7(d), we plot the $\xi = 0.02$, 0.2, 1, 2 cross sections divided by the $\xi = 1$ cross section. In both the $b\bar{b}Z^0Z^0$ and the $b\bar{b}H^0Z^0$ modes, the cross sections are weakly dependent on the ξ parameter. In the h quark mass range of 100–500 GeV/c^2, the change in the ξ parameter causes no more than a 10% change in the $b\bar{b}Z^0Z^0$ cross section and no more than a 25% change in the $b\bar{b}H^0Z^0$ cross section. Therefore, reasonable changes in the ξ parameter should not significantly impact the mass reach capability at the Fermilab Tevatron. In the remainder of this paper, we restrict our analysis to $\xi = 1$.

Effect of Higgs boson mass on cross sections. In Fig. 8, we plot the $b\bar{b}Z^0Z^0$ and $b\bar{b}H^0Z^0$ cross sections for three choices of the Higgs boson mass: $M_H = 115$, 150, and 175 GeV/c^2. At tree level, the $b\bar{b}Z^0Z^0$ cross section depends on the Higgs boson mass through the width of the h quark. In Fig. 8(a) a heavier Higgs boson leads to an enhancement in the $b\bar{b}Z^0Z^0$ cross section. This can be understood as a suppression of the $H^0 d_i$ decay channel in the h quark branching ratio [see Fig. 3(b)].

In the $b\bar{b}H^0Z^0$ cross section the Higgs boson is taken as an "external particle" in the Feynman diagrams. Therefore, the Higgs boson mass enters the cross section through the phase space integration and the expression for the h quark width. In Fig. 8(b) one observes that, by reducing the Higgs boson mass to 115 GeV/c^2, the cross section is enhanced for the mass range of 100–300 GeV/c^2. On the other hand, if we increase the mass of the Higgs boson to 175 GeV, the cross section is reduced in the same region. Above an h quark mass of 300 GeV/c^2, changes in the Higgs boson mass result in small changes to the $b\bar{b}H^0Z^0$ cross section. The negative correlation between the size of the $b\bar{b}H^0Z^0$ cross section and the mass of the Higgs boson below 300 GeV/c^2 follows from the suppression of phase space by the Higgs boson mass. In the remainder of this paper, we consider two Higgs boson masses, 115 GeV/c^2 and 150 GeV/c^2.

1. Signatures

In this section, we investigate final state signatures for $h\bar{h}$ pair production at the Tevatron. To facilitate the discussion, we categorize signatures based on the primary decay modes of the $h\bar{h}$ pair.

Below an h quark mass of 300 GeV/c^2, the dominant primary decay modes are the $b\bar{b}Z^0Z^0$ and $b\bar{b}H^0Z^0$ modes. Above an h quark mass of 300 GeV/c^2, each of the primary decay modes (see Fig. 6) is comparable in size. Therefore, a number of signatures arising from the decay of the $b\bar{b}Z^0Z^0$ and the $b\bar{b}H^0Z^0$ modes will be important for an $h\bar{h}$ search. Although cross sections from the other decay modes are comparable to the $b\bar{b}Z^0Z^0$ and the $b\bar{b}H^0Z^0$ modes when the h quark mass is greater than 300 GeV/c^2, signatures arising from these modes are often challenging experimentally.

We do not consider the $t\bar{b}Z^0W^-$ ($b\bar{t}Z^0W^+$), $t\bar{b}H^0W^-$ ($b\bar{t}H^0W^+$), and $t\bar{t}W^+W^-$ modes because the decaying t quark produces a b quark and another $W^\pm$ boson. As a result, signatures arising from these modes have at least two more final-state particles than the $b\bar{b}Z^0Z^0$ mode. At the Tevatron, small cross sections in conjunction with complicated event

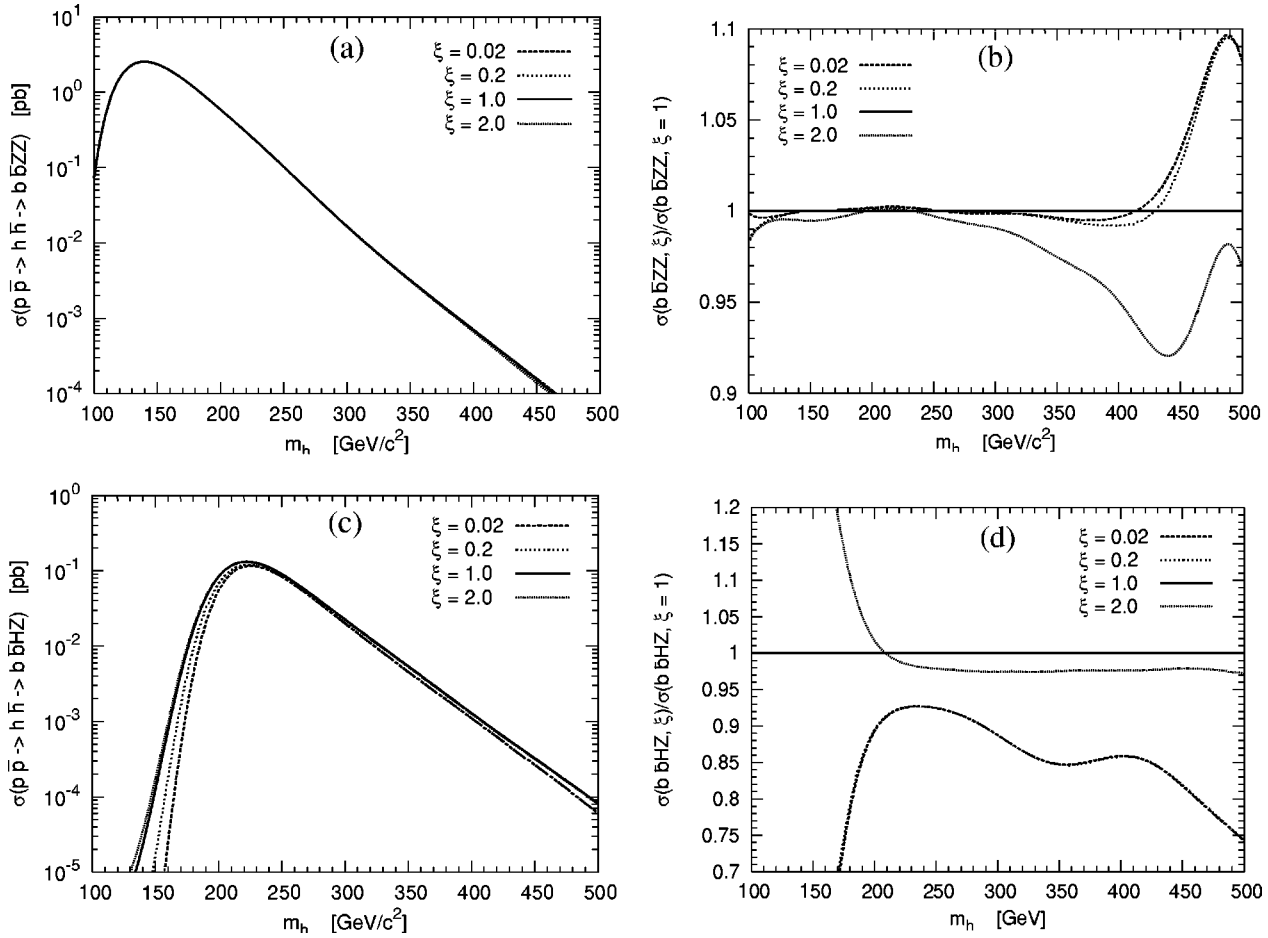

FIG. 7. Effect of the mixing parameter ξ on the "primary decay" cross sections. The curves in each of these plots correspond to four different choices of the ξ mixing parameter ($\xi=0.02$, 0.2, 1.0, and 2.0). In each of these plots, the Higgs mass is 150 GeV/c^2. (a) Plot of the cross section for $p\bar{p}\to h\bar{h}\to b\bar{b}Z^0Z^0$ as a function of h quark mass. (b) Plot of each of the $b\bar{b}Z^0Z^0$ cross sections relative to $\xi=1$ cross section. (c) Plot of the cross section for $p\bar{p}\to h\bar{h}\to b\bar{b}H^0Z^0$ as a function of h quark mass. (d) Plot of each of the $b\bar{b}H^0Z^0$ cross sections relative to $\xi=1$ cross section.

topologies, small branching ratios, and detector effects lead to little or no mass reach for these modes.

For example, signatures arising from the $t\bar{t}W^+W^-$ mode have complicated final states. In this mode, each t quark decays to a b quark and a $W^\pm$ boson: $(bW^+)_t(\bar{b}W^-)_t W^+W^-$. In our notation, the "$t$" subscript in "$(\cdot)_t$" indicates that the quantities enclosed in the parentheses have an invariant mass of the top quark, m_t. Each of the 4 $W^\pm$ bosons decays to either a quark/anti-quark pair (*hadronically*) or a charged lepton/neutrino pair (*leptonically*). In the detector the quark/anti-quark pair hadronize into two jets (jj), and the charged lepton/neutrino pair manifest as a lepton [38] and missing transverse energy ($l^\pm \not{E}_T$). Two possible final state signatures are "$b\bar{b}(jj)_W(jj)_W(jj)_W(jj)_W$" and "$b\bar{b}l^-l^+l^-l^+\not{E}_T$." The multijet signature has a complicated event topology. The final state contains two jets associated with b quarks and 8 jets arising from hadronization of light quarks. In order to reconstruct the $h\bar{h}$ parentage of this signature, one would need excellent dijet mass resolution to overcome combinatoric challenges. The fully leptonic signature suffers from small branching ratios; in addition, the presence of multiple uncorrelated neutrinos makes it cumbersome to reconstruct the parentage of the final state leptons. Other signatures arising from the $t\bar{t}W^+W^-$ mode suffer from a combination of the challenges outlined in the *full-jets* and the *fully leptonic* signatures.

In addition to the charged-current decay modes of the $h\bar{h}$, we do not consider signatures arising from the $b\bar{b}H^0H^0$ mode. Although the 6 b quark signature arising from the decay of each Higgs boson to b quarks is interesting, the $b\bar{b}H^0Z^0$ mode has a larger cross section and it leads to cleaner signatures.

At the Tevatron, the most promising channels for the discovery of a down-type isosinglet quark are the $b\bar{b}Z^0Z^0$ and the $b\bar{b}H^0Z^0$ channels. These decay channels arise from the decay of each of the h quarks via a tree-level flavor-changing neutral interaction (mediated by H^0 or Z^0) to a b quark. Jets associated with hadronized b quarks in the final state are powerful objects for analysis thanks to the b-jet identification capabilities at both detector facilities (CDF and DØ).

To obtain a more realistic description of an $h\bar{h}$ event at the Tevatron, we decay the gauge bosons in the $b\bar{b}Z^0Z^0$ and

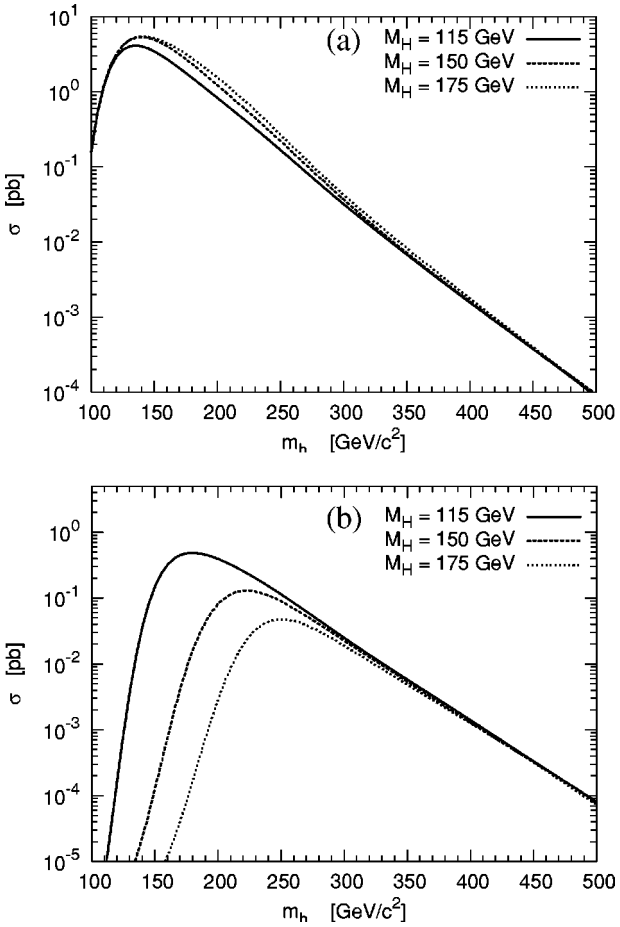

FIG. 8. Effect of the Higgs boson mass, M_H, on the primary decay cross sections. In each of these plots the mixing parameter, ξ, is fixed at 1, and the curves correspond to different Higgs boson masses (M_H=115, 150, 175 GeV/c^2). (a) Cross sections for $p\bar{p} \rightarrow h\bar{h} \rightarrow b\bar{b}Z^0Z^0$ as a function of h quark mass, and (b) cross section of $p\bar{p} \rightarrow h\bar{h} \rightarrow b\bar{b}H^0Z^0$ as a function of h quark mass.

$b\bar{b}H^0Z^0$ channels. We generate unweighted events for each of these primary decay modes, and we decay the gauge bosons to "final-state" SM particles (leptons, quarks, and gluons). When a Z^0 or an H^0 boson is decayed, we introduce a Gaussian smear on the reconstructed mass of the decay pair to approximate detector resolution effects. We take the dijet mass resolution, $\sigma(M_{jj})/M_{jj}$, of a jet pair to be 10% [39,40]. The energy resolution and transverse momentum resolution from run I of the CDF detector are used to define the dilepton mass resolution from electrons and muons [41]. Using the *signal* events, we determine the fraction of events that pass a set of detection cuts. From this fraction and the $b\bar{b}Z^0Z^0$ and $b\bar{b}H^0Z^0$ cross sections, the cross section of $h\bar{h}$ events decaying to a particular signature is determined.

In Table III we present the angular and transverse momentum cuts imposed on the events. These cuts are applied at the parton level; the quarks and gluons have not been allowed to hadronize. In our notation, "l" and "j" refer to a light charged lepton ($l=e$ or μ) and a jet ($j=u$, c, d, s, g), respectively.

TABLE III. Cuts applied to "final state" partons. l refers to either of the "light" charged leptons, e or μ. j refers to the light quarks and gluon—all of which would hadronize to form a jet. Using the "1" and "2" subscripts, we distinguish between b quarks arising from the primary decay of the h quark (b_1) and from the subsequent decay of massive gauge bosons (b_2).

Parameter	Minimum value	Maximum value
η_b, η_l, η_j	-3.0	3.0
$p_T^{b_1}$	25.0	–
p_T^l, p_T^j, $p_T^{b_2}$	10.0	–
$\Delta R(i,k)$	0.4	–

In addition to the cuts delineated in Table III, dijet and dilepton mass cuts are applied. In signatures where a Z^0 boson decays to either a charged-lepton pair or a jet pair, the reconstructed mass of that pair should be close to the mass of the Z^0 boson. Therefore, we require the mass of a dijet/dilepton pair be within $\pm(0.1\times M_Z)$. Complications may arise when more than two charged leptons or two jets are in the final state. In such instances, we define "Z^0-like" lepton or jet pairs as those with mass closest to the Z^0 mass. In analogy to the Z^0 case, we impose a dijet reconstruction cut on the b jet decay products of the H^0 boson. Also, if a Higgs boson decays to a $b\bar{b}$ pair, there will be at least 4 b jets in the final state—two b quarks from the decay of the h quarks and two b quarks from the Higgs boson decay. Rather than requiring each b jet to have a transverse momentum greater than 25 GeV/c, we require that at least two *non* "H^0-like" b jets have a transverse momentum greater than 25 GeV/c. The remaining b jets must have a transverse momentum greater than 10 GeV/c.

We also require additional cuts on the reconstructed h quark mass. For both the $b\bar{b}Z^0Z^0$ and the $b\bar{b}H^0Z^0$ modes, the h quark mass can be reconstructed from the appropriate b jet and gauge boson combinations. We constrain the invariant mass of a b quark and one of the Z^0-like or H^0-like final-state particle pairs to be equal (within resolution) to the invariant mass of the other b quark and gauge boson decay products. In addition, each of these "h quark legs" must equal (within resolution) the desired h quark mass (e.g. 200, 250, or 300 GeV/c^2). If one of the gauge bosons cannot be reconstructed (e.g. Z^0 decays to neutrinos), then the invariant mass of one of the b quarks and the other *reconstructible* Z^0-like decay products must be equal (within resolution) to the h quark mass.

With a set of formal cuts in place, we investigate specific final-state signatures arising from the $b\bar{b}Z^0Z^0$ and $b\bar{b}H^0Z^0$ channels. In Table IV we list five signatures for the $b\bar{b}Z^0Z^0$ mode and three signatures for the $b\bar{b}H^0Z^0$ mode. We consider signatures arising from Z^0 decays to a jet pair (jj), a b-jet pair (bb), a neutrino pair (missing transverse energy, $\not{E}_T$), and a pair of "light" charged leptons ($l=e$, μ). Signatures resulting from the decay of the Higgs boson to a b-jet pair are also considered. The cross sections contained in Table IV do not account for b-tagging efficiencies ($\epsilon_b = 100\%$). In Sec. IV D 2 we loosen this constraint to deter-

TABLE IV. The signal cross section (in fb) for $h\bar{h}$ pair production and subsequent decay into 7 final-state signatures. We use the "$(\cdot)_Z$" notation to indicate that the quantities enclosed in the parentheses should have an invariant mass equal to the Z^0 boson mass. The cross sections are presented for three choices of the h quark mass ($m_h=200$, 250, and 300 GeV/c^2) and for two choices of the Higgs boson mass ($M_H=115$ and 150 GeV/c^2). These cross sections assume perfect b-jet tagging efficiencies, $\epsilon_b=100\%$.

Signature	σ (fb)			σ (fb)		
m_h (GeV/c^2)	200	250	300	200	250	300
M_H (GeV/c^2)	115	115	115	150	150	150
$bb(jj)_Z(jj)_Z$	50	13	1.9	79	18	0.90
$bb(jj)_Z(l^+l^-)_Z$	19	4.9	0.72	28	6.4	0.30
$bb(jj)_Z\not{E}_T$	90	23	3.2	140	32	1.5
$bb(l^+l^-)_Z\not{E}_T$	15	4.0	0.55	26	5.6	0.29
$bb(bb)_Z\not{E}_T$	29	7.3	1.0	44	9.4	0.45
$bb(bb)_H(jj)_Z$	46	15	2.5	4.9	3.4	0.43
$bb(bb)_H(l^+l^-)_Z$	7.9	2.9	0.45	0.74	0.59	0.080
$bb(bb)_H\not{E}_T$	37	12	1.9	4.0	2.3	0.36

mine estimates of the h quark mass reach at the Tevatron.

As seen in Table IV, the most promising decay signatures in the $b\bar{b}Z^0Z^0$ channel are $b\bar{b}(jj)_Z(jj)_Z$, $b\bar{b}(jj)_Z(\not{E}_T)_Z$, and $b\bar{b}(jj)_Z(l^+l^-)_Z$. These decay signatures benefit from at least one of the Z^0 bosons decaying hadronically. The mode in which both Z^0 bosons decay to light quarks (full-jets mode) appears to provide the best reach in h quark mass. The $b\bar{b}(jj)_Z(\not{E}_T)_Z$ and $b\bar{b}(jj)_Z(l^+l^-)_Z$ signatures are relatively clean with slightly diminished signal. If the h quark mass is 250 GeV/c^2 and the mass of the Higgs boson is 150 GeV/c^2, one expects to produce (18, 180) $bb(jj)_Z(jj)_Z$ events, (6.4, 64) $bb(jj)_Z(l^+l^-)_Z$ events, and (32, 320) $bb(jj)_Z\not{E}_T$ events in (1, 10) fb^{-1} of data at the Tevatron. Many of the $b\bar{b}Z^0Z^0$ signatures are interesting and are similar to the signatures of $t\bar{t}$ production at the Tevatron. In Sec. IV D 2 we find that some of these signatures are closely related to the $t\bar{t}$ production signal, resulting in large backgrounds.

Next, we consider final state signatures arising from the $b\bar{b}H^0Z^0$ channel. In this mode the Higgs boson is produced via the tree-level FCNC decay of the h quark. Since the strength of the coupling to the h quark is proportional to the product of the flavor-changing interaction and the mass of the h quark (see Fig. 1), the Higgs boson coupling to the h quark may be sizable. This leads to an intriguing scenario in which the discovery of an isosinglet quark may lead to the discovery of the Higgs boson. We consider signatures arising from the decay of the Higgs boson to b quarks. Decays of the Higgs boson to $W^\pm$ pairs lead to complicated signatures that are not ideal for an h search at the Tevatron.

In Table IV, we consider three signatures arising from the $b\bar{b}H^0Z^0$ channel. The Z^0 boson decays to either a quark/antiquark pair, a pair of charged leptons, or a pair of neutrinos. As discussed above, jets in the final state result from the hadronization of the light quarks, and missing transverse energy ($\not{E}_T$) results from the decay of a Z^0 boson to neutrinos.

As expected, the branching ratio of the Higgs boson to a b quark pair is significantly reduced as one increases the Higgs boson mass from 115 GeV/c^2 to 150 GeV/c^2. Signatures arising from the $b\bar{b}H^0Z^0$ channel have the most reach when there is a *light* Higgs boson. In addition, the $bb(bb)_H(jj)_Z$ and the $bb(bb)_H\not{E}_T$ signatures have much larger cross sections than the $bb(bb)_H(l^+l^-)_Z$ signature. If the h quark mass is 250 GeV/c^2 and the Higgs boson mass is 115 GeV/c^2, one expects to produce (15, 150) $bb(bb)_H(jj)_Z$ events and (12, 120) $bb(bb)_H\not{E}_T$ in (1, 10) fb^{-1} of data at the Fermilab Tevatron.

2. Backgrounds

In the previous section we presented a number of $h\bar{h}$ signatures and their expected tree-level cross sections at the Tevatron. To ascertain the h quark mass reach at the Tevatron, we need to understand the backgrounds associated with these signatures (see Table IV).

We use the software package MADEVENT [42] to study the SM backgrounds for these signatures. MADEVENT generates and calculates the *tree-level* contributions to a given process (parton-level calculation) using helicity amplitude methods [43]. We do not consider one-loop contributions to the background. Although FCNCs occur at one loop in the SM, we expect their contribution to the background to be small. If one includes one-loop processes in the SM background calculation, the one-loop contribution to the ISVLQ model should be included in the signal calculation.

At the parton level, each of the $h\bar{h}$ signatures contains six final state particles (quarks and leptons). Although MADEVENT can generate the diagrams and associated matrix elements for a signature containing six "final-state" particles, the evaluation of some matrix elements is computationally intractable. In particular, the quantum chromodynamic backgrounds to the $bb(jj)_Z(jj)_Z$ and the $bb(bb)_H(jj)_Z$ signatures consist of an enormous set of tree-level diagrams that overwhelm most computing clusters. Therefore, when com-

TABLE V. Standard model background to the $h\bar{h}$ pair production signatures outlined in Sec. IV D 1. The SM background cross sections are presented for a Higgs boson mass of 115 and of 150 GeV/c^2. A b-jet tagging efficiency of 50% is used and at least 1 or 3 b tags are required for signatures containing 2 or 4 b jets, respectively. In the "EW order" columns we indicate the order of each of the electroweak calculations. A number in either of these columns indicates the number of electroweak vertices in the background calculation, the "FT" indicates that the calculation is a full tree-level calculation, and the asterisk indicates that the background is forced to produce massive gauge bosons before decaying to the indicated signature.

Signature	σ_{bkgrnd} (fb)			σ_{bkgrnd} (fb)			EW order	
M_h (GeV/c^2)	200	250	300	200	250	300	(calc)	(uncalc)
M_H (GeV/c^2)	115	115	115	150	150	150		
$bb(jj)_Z(jj)_Z$	110	56	16	110	57	15	2,4*	0,>4
$bb(jj)_Z(l^+l^-)_Z$	0.023	0.0098	0.0044	0.024	0.010	0.0043	2,4*	>4
$bb(jj)_Z\not{E}_T$	1.8	0.57	0.30	1.3	0.57	0.53	2,4*	>4
$bb(l^+l^-)_Z\not{E}_T$	8.4	6.1	2.6	8.4	6.1	2.6	FT	
$bb(bb)_Z\not{E}_T$	0.023	0.014	0.0081	0.022	0.014	0.0079	2,4*	>4
$bb(bb)_H(jj)_Z$	0.059	0.0023	0.0010	0.0025	0.0019	0.00091	2,4*	0,>4
$bb(bb)_H(l^+l^-)_Z$	0.0035	0.0013	0.00047	0.0026	0.0015	0.00047	2,4*	>4
$bb(bb)_H\not{E}_T$	0.021	0.014	0.0087	0.013	0.013	0.0090	2,4*	>4

putationally feasible, we use MADEVENT to calculate the SM background to the $h\bar{h}$ signatures. The order of the background calculation will accompany all estimates of the background cross sections. For signatures like the $bb(jj)_Z(jj)_Z$, in which the matrix elements for the backgrounds are not calculable using current technology, one would need to use approximate methods or to measure the background directly from the Tevatron data.

For each signature, we require background processes to pass the cuts outlined in Table III and the invariant mass cuts discussed in Sec. IV D 1. As with the signal events, we assume that at the Tevatron the dijet mass resolution can be approximated by a Gaussian distribution with a resolution of 10% of the invariant mass. The dijet and dilepton cuts and the cuts in Table III are designed to reduce the size of the background. For example, the hard cut on the transverse momentum of b quarks from the primary h quark decay ($p_T^b > 25$ GeV/c^2) in conjunction with the jet separation cut ($\Delta R > 0.4$) helps reduce backgrounds from gluon splitting to $b\bar{b}$. The dijet mass cuts help reduce QCD backgrounds that duplicate our $h\bar{h}$ production signatures.

In Table V, we present the results of our SM background calculation for each of the signatures listed in Table IV. For the SM background calculations we assume a b-jet tagging efficiency of 50%; if a b jet is *not* tagged, then it is treated as a jet (j). For signatures containing 2 or 4 b jets, we require at least 1 or 3 b-jet tags, respectively. As discussed above, we are unable to calculate the matrix element of the backgrounds for some signatures because of computational limitations. In columns four and five of Table V, we indicate the electroweak order of the background for which we were able and unable to calculate. In these columns, a number indicates the number of electroweak vertices in the background calculation, the "FT" indicates that the calculation is a full tree-level calculation, and the asterisk indicates that the background is forced to produce massive gauge bosons before decaying to the indicated signature. For example, we calculated the $bb(jj)_Z(l^+l^-)_Z$ background originating from diagrams with two electroweak vertices and with four electroweak vertices. The background with two electroweak vertices includes diagrams where the jets do not come from Z^0 decay. The background with four electroweak vertices includes all $b\bar{b}(jj)_Z(l^+l^-)_Z$ signatures that arise from $b\bar{b}\mathcal{X}\mathcal{X}$, where $\mathcal{X}$ is a massive gauge boson, $\mathcal{X}=Z^0$, $W^\pm$, or H^0.

For most of the signatures discussed in Sec. IV D 1, the SM background appears to be manageable when compared to the signal cross sections (see Table IV). The notable exceptions are the $bb(jj)_Z(jj)_Z$ and the $bb(l^+l^-)_Z\not{E}_T$ signatures. The large backgrounds for these signatures (relative to the other signatures) can be traced to top quark pair production. At the Tevatron, $t\bar{t}$ production, like the $h\bar{h}$ production, proceeds via quark/anti-quark annihilation and gluon-gluon fusion. Once the $t\bar{t}$ are produced, each top quark decays to a b and a W^+. Subsequent decay of the $W^\pm$ bosons results in the following three signatures: "$b\bar{b}(jj)_W(jj)_W$" (full jets), "$b\bar{b}(jj)_W l^\pm\not{E}_T$" (semi-leptonic), and "$b\bar{b}l^+l^-\not{E}_T$" (fully leptonic). We use the "$(\cdot)_W$" notation to indicate that the quantities enclosed in the parentheses have an invariant mass equal to the $W^\pm$ boson mass.

If the dijet mass resolution at the Tevatron were perfect, then a jet pair from a $W^\pm$ decay and a jet pair from a Z^0 decay would always be distinguishable. However, the dijet mass resolution at the Tevatron is not perfect; therefore, a fraction of the $t\bar{t}$ events decaying to the full-jets mode will mimic the $bb(jj)_Z(jj)_Z$ signature. We find that for a Higgs boson mass of 150 GeV/c^2 and an h quark mass of 250 GeV/c^2, the background to the signature $bb(jj)_Z(jj)_Z$ is 57 fb. The purely QCD component of this background (denoted "0" in Table V) was not calculated. Although one expects the invariant mass cuts to substantially reduce this background, it is unlikely that it will be negligible. Thus we conclude that the $bb(jj)_Z(jj)_Z$ signature is background lim-

ited and that other $h\bar{h}$ signatures will provide a better h quark mass reach. However, if nature contains an h quark with a mass less than ~ 250 GeV/c^2, this signature will provide a channel to measure the mass of the h quark (h quark mass peak).

The $bb(l^+l^-)_Z\not{E}_T$ signature also has a sizable $t\bar{t}$ background component. When a $t\bar{t}$ event decays to the fully leptonic mode, the invariant mass of the two charged leptons *may* be close to the mass of the Z^0 boson. One concludes that, like the $bb(jj)_Z(jj)_Z$ signature, the h quark mass reach of the $bb(l^+l^-)_Z\not{E}_T$ signature is diminished because of the background.

The $b\bar{b}(jj)_Z(l^+l^-)_Z$ and $b\bar{b}(jj)_Z\not{E}_T$ signatures provide clean alternatives to the full jets signature. Unlike the $bb(jj)_Z(jj)_Z$ signature, the $b\bar{b}(jj)_Z\not{E}_T$ signature is not afflicted by a large $t\bar{t}$ background. The semi-leptonic decay of a $t\bar{t}$ event can duplicate the $b\bar{b}(jj)_Z\not{E}_T$ signature if the dijet mass is close to the Z^0 mass and the charged lepton is undetected. In Table V, we include this and other backgrounds to the $b\bar{b}(jj)_Z\not{E}_T$ signature in which a charged lepton from the decay of a $W^{\pm}$ is undetected. In order to determine the ''undetected lepton'' background, we assume that this background originates from events in which the charged lepton travels through an uninstrumented region of the detector [44]. The ''lost-lepton'' background is also included in the $b\bar{b}(l^+l^-)_Z\not{E}_T$, $b\bar{b}(bb)_Z\not{E}_T$, and $b\bar{b}(bb)_H\not{E}_T$ signatures. Although other experimental issues, like jet energy mismeasurement of QCD jets, are likely to increase the background, we do not include these in our calculation.

The $b\bar{b}(jj)_Z(l^+l^-)_Z$ signature also avoids large $t\bar{t}$ backgrounds. The semi-leptonic decay of a $t\bar{t}$ event can mimic this signature if the dijet mass is Z^0-like and the detector spuriously identifies an additional lepton. The dilepton mass of the real and spurious charged leptons must be Z^0-like. This component of the background is expected to be small; therefore, we do not include it in the background estimate.

Since the $b\bar{b}(jj)_Z(l^+l^-)_Z$ and the $b\bar{b}(jj)_Z\not{E}_T$ are clean signatures with small backgrounds, we expect these modes to provide the greatest reach at the Tevatron. In (1, 10) fb^{-1} of data, the highest h quark mass accessible by the $b\bar{b}(jj)_Z(l^+l^-)_Z$ and the $b\bar{b}(jj)_Z\not{E}_T$ signatures are (230, 290) GeV/c^2 and (270, 320) GeV/c^2, respectively.

While the $b\bar{b}Z^0Z^0$ mode is likely to provide the best reach for an h quark search, the $b\bar{b}H^0Z^0$ mode provides an opportunity to discover the Higgs boson in conjunction with the h quark. If nature favors a light Higgs boson (e.g. $M_H=115$ GeV/c^2), the dominant branching ratio of the Higgs boson is the $b\bar{b}$ mode, $BR(H^0\rightarrow b\bar{b})=73.2\%$. However, if the mass of the Higgs boson is larger than current electroweak best fits [45], the $b\bar{b}H^0Z^0$ mode is less powerful. For example, at a Higgs boson mass of 150 GeV/c^2, the Higgs boson branching ratio to $b\bar{b}$ is 17.6%.

Unlike many of the $b\bar{b}Z^0Z^0$ signatures, the $b\bar{b}H^0Z^0$ signatures do *not* suffer from the large $t\bar{t}$ background. The reduction in the $t\bar{t}$ background is primarily because of the $b\bar{b}$ signature from the Higgs boson decay ($W^{\pm}$ cannot decay to a $b\bar{b}$ pair). Although these signatures have low SM backgrounds, b-tagging efficiencies will reduce the expected signal cross section.

Standard model background to each of the three $b\bar{b}H^0Z^0$ signatures is small (see Table V). Because of computational limitations, the pure QCD component of the $b\bar{b}(bb)_H(jj)_Z$ background (denoted ''0'' in Table V) was not calculated. As with the background for the $b\bar{b}(jj)_Z(jj)_Z$ signature, the QCD component of the $b\bar{b}(bb)_H(jj)_Z$ signature will need to be measured from the data. It is unlikely that the background from these processes will be large. Assuming a b-tagging efficiency of 50% and requiring that three of the four b jets is tagged, for a Higgs boson mass of 115 GeV/c^2 one expects the mass reach in the $b\bar{b}(bb)_H\not{E}_T$ mode to be (230, 290) GeV/c^2 in (1, 10) fb^{-1} of data. Moreover, because the background to the $b\bar{b}(jj)_H(jj)_Z$ signature is not expected to be large, we expect for a Higgs boson mass of 115 GeV/c^2 the h mass reach of this mode to be $\sim$(220, 270) GeV/c^2.

V. $h\bar{h}$ PRODUCTION AND DECAY AT THE LHC

At the c.m. energy of the CERN LHC ($\sqrt{s}=14$ TeV), $h\bar{h}$ pair production is dominated by the gluon-gluon fusion subprocess. Contributions from subprocesses in which a valence quark from one proton and its anti-particle from the other proton (sea quark) annihilate via the strong interactions are important but sub-dominant to the gluon-gluon fusion.

For the LHC we consider the same primary decay channels of the $h\bar{h}$ pair as at the Tevatron: $t\bar{t}W^+W^-$, $b\bar{b}Z^0Z^0$, $b\bar{b}H^0H^0$, $t\bar{b}W^-Z^0$, $b\bar{b}H^0Z^0$, and $t\bar{b}W^-H^0$. We also impose the same set of loose cuts on the primary decay products of the h quark (see Table II). This ensures that b quarks produced from the primary decay of the $h\bar{h}$ pair conform to *basic* geometry and event selection requirements of the detectors.

The cross sections for $h\bar{h}$ production and (primary h quark) decay at the LHC are shown in Fig. 9. In this figure, the new mixing parameter, ξ, is set to 1, the Higgs boson mass, M_H, is set to 150 GeV/c^2, and the h quark mass, m_h, runs from 100 to 3000 GeV/c^2. The cross sections for the $h\bar{h}$ primary decay modes at the LHC are roughly two orders of magnitude larger than the corresponding cross sections at the Tevatron. Below 300 GeV/c^2, the $b\bar{b}Z^0Z^0$ mode is once again the dominant primary decay mode of $h\bar{h}$ pair production. Above an h quark mass of 300 GeV/c^2, each of the primary decay cross sections is comparable; however, the decay modes with at least one charged-current decay of the h quark tend to be larger.

At the LHC the cross sections for each of the three charged-current primary decay modes are significant, unlike those at the Tevatron. For an h quark mass of 500 GeV/c^2 and a mixing parameter $\xi=1$, the LHC should produce

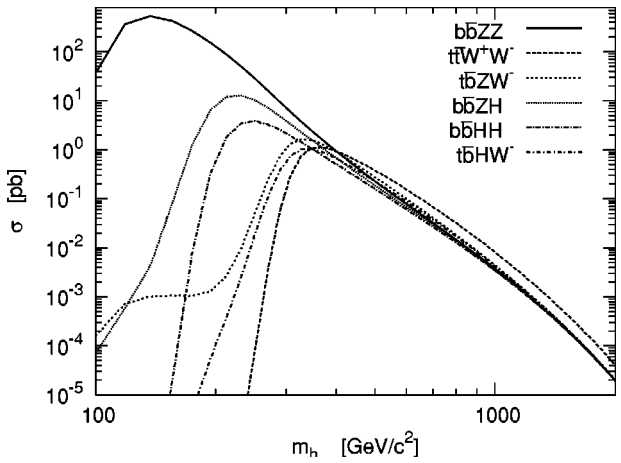

FIG. 9. Cross sections for $h\bar{h}$ production and primary decay at the CERN LHC. The Higgs boson mass is $M_H=150$ GeV/c^2, the new mixing parameter $\xi=1$, and $Q=2m_h$.

$\sim$20 000 $h\bar{h}$ events decaying to the $t\bar{t}W^+W^-$ mode in 100 fb^{-1} of data. The charged-current mode of $h\bar{h}$ decay is important because our parametrization of the L^d (CKM) matrix in the ISVLQ model predicts a relationship between the size of charged-current and neutral-current interactions. As discussed in Sec. IV D 2, the charged-current modes have final states that are more complicated than those encountered in FCNC decay modes. Additional complications are attributed to the decay of the top quark resulting in an additional $W^{\pm}$ boson. With additional particles in the final state, dijet mass resolution and the calculation of signature backgrounds are extremely important components for an analysis. Rather than address the charged-current modes in this paper, we defer this analysis to future research when the difficulties of the background calculation and details about dijet mass resolution and b tagging can be better resolved.

In our analysis of $h\bar{h}$ production at the Tevatron (see Sec. IV D), we found that signatures of the $b\bar{b}Z^0Z^0$ mode provide the highest h quark mass reach. We conclude that in 10 fb^{-1} of data, $h\bar{h}$ pair production can be probed up to an h quark mass of 320 GeV/c^2. At this h quark mass and for a Higgs boson mass of 150 GeV/c^2, the cross section to the $b\bar{b}Z^0Z^0$ mode ($\sigma_{bbZZ}=20$ fb) and the branching ratio to the "optimal" signatures combine to produce a handful of signal events with negligible background. Based on our study of the $b\bar{b}Z^0Z^0$ mode at the Tevatron, we infer a mass reach for this decay mode at the LHC. We assume that the branching ratios of the $b\bar{b}Z^0Z^0$ mode to *final-state* signatures and the detection of these signatures at the LHC are similar to those at the Tevatron. Therefore, at the LHC, the upper limit on the h quark mass is encountered when approximately 200 events are produced in the $b\bar{b}Z^0Z^0$ mode. The expected integrated luminosity at the LHC is 100 fb^{-1}; thus one can probe the $b\bar{b}Z^0Z^0$ cross section down to 2 fb. This corresponds to an h quark mass reach of 1100 GeV/c^2 (see Fig. 9).

VI. CONCLUSION

We have investigated an E_6-inspired extension of the standard model in which an exotic charge $-1/3$ isosinglet vectorlike quark (denoted h) interacts predominantly with the third generation of quarks. In this model, the CKM matrix is no longer unitary and it is replaced by a 3×4 matrix containing new angles and phases. The loss of CKM unitarity is accompanied by the emergence of *tree-level* flavor-changing neutral currents mediated by both Z^0 and H^0 bosons. Flavor-changing neutral-current interactions between the h quark and the b quark produce signatures of $h\bar{h}$ production accessible for detection at hadron colliders.

At the Fermilab Tevatron, we find that h quark discovery through pair production is accessible up to an h quark mass of (270, 320) GeV/c^2 in (1, 10) fb^{-1} of data. Previous b' analyses from run I of the Tevatron were used to infer that an h quark is currently excluded up to 200 GeV/c^2. The (270, 320) GeV/c^2 mass reach is attainable through the decay of the $b\bar{b}Z^0Z^0$ mode to the $b\bar{b}(jj)_Z(l^+l^-)_Z$ or the $b\bar{b}(jj)_Z\not{E}_{\mathrm{T}}$ signatures. Furthermore, primary decay of an $h\bar{h}$ pair to the $b\bar{b}H^0Z^0$ mode provides the opportunity for the discovery of the Higgs boson in conjunction with h quark discovery. The viability of the $b\bar{b}H^0Z^0$ mode at the Tevatron hinges on the branching ratio of the Higgs boson to a b quark pair.

At the CERN LHC, $h\bar{h}$ pair production is accessible through both charged-current and neutral-current decays of the h quark. In 100 fb^{-1} of data, we find that the h quark mass reach through the $b\bar{b}Z^0Z^0$ primary decay mode is 1100 GeV/c^2. To understand the reach of the charged-current primary decay modes, an analysis of potential signatures, the effect of detector limitations, and signature backgrounds is necessary. A thorough analysis of $h\bar{h}$ charged-current decay modes ($t\bar{b}W^-Z^0$, $t\bar{b}W^-H^0$, and $t\bar{t}W^+W^-$) at the LHC is deferred to future work.

ACKNOWLEDGMENTS

We thank H. Frisch, C. E. M. Wagner, and D. Morrissey for useful discussions. We also thank the University of Chicago CDF group for computing time. We are grateful to Stephen Wolbers, Igor Mandrichenko, and Margaret Greaney from the Computing Division (ISD Department) at the Fermi National Accelerator Laboratory.

[1] H. Georgi, in *Particles and Fields—1974*, edited by C. E. Carlson, AIP Conf. Proc. No. **23** (AIP, New York, 1975) p. 575; H. Fritzsch and P. Minkowski, Ann. Phys. (N.Y.) **93**, 193 (1975).

[2] F. Gürsey, P. Ramond, and P. Sikivie, Phys. Lett. **60B**, 177 (1976); Y. Achiman and B. Stech, *ibid.* **77B**, 389 (1978); Q. Shafi, *ibid.* **79B**, 301 (1978); F. Gürsey and M. Serdaroglu,

Lett. Nuovo Cimento Soc. Ital. Fis. **21**, 28 (1978); Nuovo Cimento Soc. Ital. Fis., A **65**, 337 (1981); R. Barbieri, D.V. Nanopoulos, and A. Masiero, Phys. Lett. **104B**, 194 (1981).
[3] J.L. Rosner, Comments Nucl. Part. Phys. **15**, 195 (1986).
[4] J.L. Rosner, Phys. Rev. D **61**, 097303 (2000).
[5] B. Stech and Z. Tavartkiladze, hep-ph/0311161.
[6] D. Chang and R.N. Mohapatra, Phys. Lett. B **175**, 304 (1986); Phys. Rev. Lett. **58**, 1600 (1987).
[7] J.L. Hewett and T.G. Rizzo, Phys. Rep. **183**, 193 (1989).
[8] E. Nardi, E. Roulet, and D. Tommasini, Phys. Rev. D **46**, 3040 (1992).
[9] T.G. Rizzo, Phys. Rev. D **59**, 015020 (1999).
[10] G.C. Branco and L. Lavoura, Nucl. Phys. **B278**, 738 (1986).
[11] R.W. Robinett, Phys. Rev. D **33**, 1908 (1986).
[12] B.A. Campbell, J.R. Ellis, K. Enqvist, M.K. Gaillard, and D.V. Nanopoulos, Int. J. Mod. Phys. A **2**, 831 (1987).
[13] V.D. Barger, N. Deshpande, R.J. Phillips, and K. Whisnant, Phys. Rev. D **33**, 1912 (1986); **35**, 1741(E) (1987).
[14] F. del Aguila, G.L. Kane, and M. Quiros, Phys. Lett. B **196**, 531 (1987).
[15] P. Langacker and D. London, Phys. Rev. D **38**, 886 (1988).
[16] H. Fritzsch and Z.Z. Xing, Phys. Lett. B **353**, 114 (1995).
[17] W.S. Hou and H.C. Huang, Phys. Rev. D **51**, 5285 (1995).
[18] D.E. Morrissey and C.E.M. Wagner, Phys. Rev. D (to be published), hep-ph/0308001.
[19] Y. Nir and D. Silverman, Phys. Rev. D **42**, 1477 (1990); V. Barger, M.S. Berger, and R.J.N. Phillips, *ibid.* **52**, 1663 (1995).
[20] S.L. Glashow, J. Iliopoulos, and L. Maiani, Phys. Rev. D **2**, 1285 (1970).
[21] J.A. Aguilar-Saavedra, Phys. Rev. D **67**, 035003 (2003).
[22] D. Hawkins and D. Silverman, Phys. Rev. D **66**, 016008 (2002); J.D. Bjorken, S. Pakvasa, and S.F. Tuan, *ibid.* **66**, 053008 (2002).
[23] M. Shin, M. Bander, and D. Silverman, Phys. Lett. B **219**, 381 (1989); Y. Nir and D.J. Silverman, Nucl. Phys. **B345**, 301 (1990); D. Silverman, Phys. Rev. D **45**, 1800 (1992); Int. J. Mod. Phys. A **11**, 2253 (1996).
[24] L. Lavoura and J.P. Silva, Phys. Rev. D **47**, 1117 (1993); **47**, 2046 (1993).
[25] L. Wolfenstein, Phys. Rev. Lett. **51**, 1945 (1983).
[26] Y. Nir and D. Silverman, Phys. Rev. D **42**, 1477 (1990); W.S. Choong and D. Silverman, *ibid.* **49**, 2322 (1994); D. Silverman, *ibid.* **58**, 095006 (1998).
[27] F. del Aguila, J.A. Aguilar-Saavedra, and G.C. Branco, Nucl. Phys. **B510**, 39 (1998); G.C. Branco, T. Morozumi, P.A. Parada, and M.N. Rebelo, Phys. Rev. D **48**, 1167 (1993).
[28] G. Barenboim, F.J. Botella, G.C. Branco, and O. Vives, Phys. Lett. B **422**, 277 (1998).
[29] K. Yamamoto, hep-ph/9707417; I. Kakebe and K. Yamamoto, Phys. Lett. B **416**, 184 (1998).
[30] Though an interesting scenario, a large coupling between the *h* quark and *u* or *c* quarks appears to be disfavored by bounds discussed in Sec. III B.
[31] CTEQ Collaboration, H.L. Lai *et al.*, Eur. Phys. J. C **12**, 375 (2000).
[32] A. Pukhov, E. Boos, M. Dubinin, V. Edneral, V. Ilyin, D. Kovalenko, A. Kryukov, V. Savrin, S. Shichanin, and A. Semenov, Report No. INP MSU 98-41/542, hep-ph/9908288.
[33] D. Cronin-Hennessy, A. Beretvas, and P. Derwent, Nucl. Instrum. Methods Phys. Res. A **443**, 37 (2000); M. G. Albrow, A. Beretvas, L. Nodulman, and P. Giromini, Report No. FERMILAB-TM-2071; DØ Collaboration, V.M. Abazov *et al.*, Phys. Lett. B **517**, 299 (2001)
[34] DØ Collaboration, S. Abachi *et al.*, Phys. Rev. Lett. **78**, 3818 (1997).
[35] CDF Collaboration, T. Affolder *et al.*, Phys. Rev. Lett. **84**, 835 (2000).
[36] The CDF Collaboration, F. Abe *et al.*, Phys. Rev. D **58**, 051102 (1998).
[37] Technically, for ξ parameters not of $\mathcal{O}(1)$ (e.g. $\xi=0.02$), one should reparametrize the L^d_{34} element of the L^d matrix so that the matrix parametrization is consistent.
[38] In the detector, the decay of τ leptons results in a jet signature. In this paper, we restrict our signature analysis to non-tau leptonic decays of the $W^{\pm}$ bosons.
[39] We use a 10% dijet mass resolution for both light quark hadronization and *b* quark hadronization. Although optimistic, it is expected that improved energy flow techniques will attain a resolution commensurate with this value [40].
[40] S. Lami, A. Bocci, S. Kuhlmann, and G. Latino, in Proceedings of the 9th Conference on Calorimetry in High Energy Physics (CALOR 2000), Annecy, France, 2000, Report No. FERMILAB-CONF-00/342-E; G.C. Blazey *et al.*, hep-ex/0005012; C.F. Berger *et al.*, in Proceedings of the APS/DPF/DPB Summer Study on the Future of Particle Physics (Snowmass 2001), edited by N. Graf, eConf C010630, p. 512, hep-ph/0202207; DØ Collaboration, E. Gallas, FERMILAB-CONF-02-330-E talk at 14th Topical Conference on Hadron Collider Physics (HCP 2002), Karlsruhe, Germany, 2002 Report No. FERMILAB-CONF-02-330-E; jet algorithms in run 2 at CDF, http://www-cdf.fnal.gov/physics/new/qcd/qcd_plots/jetalgo/gene.html, 2003.
[41] CDF Collaboration, T. Affolder *et al.*, Phys. Rev. D **64**, 052001 (2001).
[42] F. Maltoni and T. Stelzer, J. High Energy Phys. **02**, 027 (2003).
[43] H. Murayama, I. Watanabe, and K. Hagiwara, Report No. KEK-91-11.
[44] Although additional regions of the detector are uninstrumented (e.g. cracks between detector components, cooling instrumentation, etc.), we approximate the uninstrumented volume of the detector as to the angular region $|\eta|>3$.
[45] LEP Electroweak Working Group, http://lepewwg.web.cern.ch/LEPEWWG, 2001.